21090

NATIONAL LIBRARY
OTTAWA

BIBLIOTHÈQUE NATIONALE
OTTAWA

NAME OF AUTHOR... RAMESH, VENKATARAMANAYYA

TITLE OF THESIS... DIRECT SIMULTANEOUS MEASUREMENT OF ROTATIONAL AND TRANSLATIONAL ACCOMMODATION COEFFICIENT

UNIVERSITY... UNIVERSITY OF ALBERTA

DEGREE FOR WHICH THESIS WAS PRESENTED... PH.D.

YEAR THIS DEGREE GRANTED... 1974

Permission is hereby granted to THE NATIONAL LIBRARY OF CANADA to microfilm this thesis and to lend or sell copies of the film.

The author reserves other publication rights, and neither the thesis nor extensive extracts from it may be printed or otherwise reproduced without the author's written permission.

(Signed)... V. Ramesh

PERMANENT ADDRESS:

207, 57th - 112 St

EDMONTON - ALTA

DATED... 24th JAN ... 1974

NL-91 (10-68)

THE UNIVERSITY OF ALBERTA

DIRECT SIMULTANEOUS MEASUREMENT OF ROTATIONAL AND TRANSLATIONAL ACCOMMODATION COEFFICIENTS

BY

© RAMESH VENKATARAMANAYYA

A THESIS

SUBMITTED TO THE FACULTY OF GRADUATE STUDIES AND RESEARCH

IN PARTIAL FULFILLMENT OF THE REQUIREMENTS FOR

DOCTOR OF PHILOSOPHY DEGREE

DEPARTMENT OF MECHANICAL ENGINEERING

EDMONTON, ALBERTA

SPRING 1974

THE UNIVERSITY OF ALBERTA

FACULTY OF GRADUATE STUDIES AND RESEARCH

The undersigned certify that they have read, and recommend to the Faculty of Graduate Studies and Research, for acceptance, a thesis entitled "DIRECT SIMULTANEOUS MEASUREMENT OF ROTATIONAL AND TRANSLATIONAL ACCOMMODATION COEFFICIENTS" submitted by RAMESH VENKATARAMANAYYA in partial fulfillment of the requirements for the Doctrate Degree.

David Marsden

Supervisor

Date 9 Jan. 1974

ABSTRACT

When molecules of a low density diatomic gas strike a solid surface, both the translational energy and the internal energy modes of rotation and vibration will contribute to the energy exchange that occurs.

The experimental apparatus described here uses the electron beam fluorescence detector to measure simultaneously both the rotational and the translational energy accommodation coefficient of room temperature nitrogen reflecting from a heated solid surface. Nickel, silver, gold and stainless steel surfaces were tested in a bakeable ultrahigh vacuum system built to provide a clean vacuum environment for control of the solid surface composition.

Theoretical studies indicate that the accommodation coefficient of rotational energy should be less than that for translational energy, and this is confirmed by experimental results.

Results show that for the pure metals - nickel, silver and gold, the translational accommodation coefficients α_T are 0.5, 0.4 and 0.2 respectively at 400°K; and the variation of α_T with the increase in surface temperature, T_s, is given approximately by the equation:

$$d\alpha_T/dT_s = -13.7278 \times 10^{-4} + 2.6042 \times 10^{-4}/\mu$$

where μ is the ratio of the masses of the gas molecule and the solid atom. For the alloy stainless steel, the translational coefficient

decreases sharply with increase in surface temperature.

Based on the above equation, an empirical relationship has been developed for translational accommodation coefficient α_T in the form

$$\alpha_T = \frac{d\alpha_T}{dT_s} T_s + \text{constant}$$

where the constant of integration has been adjusted by fitting the equation to the best available experimental data. The resulting closed form solution for α_T not only gives a good description of the results obtained in the present work but also predicts good results for a wide range of gas-surface combinations and conditions.

The results also show that the rotational coefficient, α_R, is approximately 0.5 for stainless steel and 0.15 for nickel and gold. There is very little variation with surface temperature for these materials. For silver, the rotational coefficient increases from about 0.03 at 400°K to 0.2 at 700°K.

In addition to being the only known direct method of measurement of the rotational accommodation coefficient, the system used here offers an advantage over some previous methods of translational accommodation measurement in that there are few restrictions on solid surface temperature or composition.

ACKNOWLEDGEMENTS

The author wishes to extend his deep appreciation to Dr. D.J. MARSDEN for his guidance and supervision of this thesis. The financial assistance of the National Research Council is gratefully acknowledged.

Thanks are extended to the members of the mechanical and electronic shops and to Mrs. June Hole for typing this thesis.

The author wishes to take this opportunity to extend his most heartfelt thanks to his wife for her extreme patience during these long years.

TABLE OF CONTENTS

		Page
CHAPTER I	INTRODUCTION	1
CHAPTER II	EXPERIMENTAL APPARATUS	13
	2.1 Vacuum System	13
	2.2 Chamber A	13
	2.3 Chamber B	15
	2.4 Chamber C	17
	2.5 Pressure Measurement	18
	2.6 Temperature Measurement	18
	2.7 Optics	19
CHAPTER III	EXPERIMENTAL PROCEDURE	21
	3.1 Surface Target Preparation	21
	3.2 Introduction of Test Gas	22
	3.3 Determination of Accommodation Coefficients	24
CHAPTER IV	THEORY	25
	4.1 Geometrical Considerations	25
	4.2 Electron Beam Measurements	29
	4.3 Translational Accommodation Coefficients	32
	4.4 Rotational Accommodation Coefficients	35

		Page
CHAPTER V	RESULTS AND DISCUSSION	43
	5.1 Rotational Accommodation Coefficient	43
	5.2 Estimation of Accuracy of Measured Rotational Accommodation Coefficient	46
	5.3 Translational Accommodation Coefficient	51
	5.4 Estimation of Accuracy of Measured Translational Accommodation Coefficient	59
	5.5 Surface Conditions	61
CHAPTER VI	CONCLUSIONS	64
BIBLIOGRAPHY		66
APPENDIX		70

LIST OF TABLES

Table		Page
1.	Theoretical Values of Translational and Internal Accommodation Coefficients	7
2.	Theoretical Values of Line Intensities at Room Temperature	38
3.	Predicted Accommodation Coefficients for Monatomic Gases	56
4.	Typical Analysis of Surface Material Composition	62
5.	Chemical Adsorption	63
6.	Wavelength of Peaks of the R-branch	73

LIST OF FIGURES

Figure		Page
1.	Schematic Diagram of the Experimental Apparatus	14
2.	Target Mounting Details	16
3.	Schematic Diagram of the Optical System	20
4.	Partial Pressure of Nitrogen	23
5.	Details of the Detector Geometry	27
6.	Spectrometer Scan of the R-Branch of the $N_2^+(0,0)$ band	30
7.	Typical Line Intensities in the Background and Reflected Molecules	33
8.	Variation of Rotational Accommodation Coefficient of Nickel, Silver and Gold with Surface Temperature	44
9.	Variation of Theoretical Error Limits of Accommodation Coefficients of Stainless Steel with Surface Temperature	48
10.	Variation of Translational Accommodation Coefficient of Nickel, Silver and Gold with Surface Temperature	52
11.	Mechanism of Fluorescence	71

LIST OF SYMBOLS

A'	Area of the orifice between chambers A and B
B	rotational constant corresponding to the lowest vibrational level
c	velocity of gas molecules reflected from the target
C_1	free molecular conductance of the orifice between chambers A and B
C_2	free molecular conductance of the bypass between chambers A and B
E_1	energy of the incident gas molecules
E_r	energy of the reflected gas molecules
E_s	ideal energy of the gas molecules at the temperature of the surface
f_r	Maxwellian velocity distribution function of the reflected molecules
$[G]$	function of rotational quantum number and temperature (equation 4.11)
h	Planck's constant
$I(K)$	line intensity of light at rotational level K
I_1	Σ I(K'), bypass valve open
I_2	Σ I(K'), bypass valve closed
I_R	contribution to line intensity of the reflected molecules
I_B	contribution to line intensity of the background molecules

$I_{table}(K)$ line intensity at rotational level K of room temperature gas given in Table 2

J rotational quantum number - includes electron spin

k Boltzmann's constant

K' rotational quantum number of the upper electronic state of the nitrogen ion - excludes electron spin

K'' rotational quantum number of the lower electronic state of the nitrogen ion - excludes electron spin

M molecular weight of gas

M_s atomic weight of material of the surface

n number density of gas molecules along the electron beam

n_a contribution of reflected molecules to number density

n_b contribution of background molecules to number density

n_A number density of gas molecules in chamber A

n_B number density of gas molecules in chamber B

n_r number density of reflected molecules

N total number of molecules

N(c) number of molecules with velocity c

N_J number of molecules in rotational level J

n_1 number density of molecules along the electron beam - bypass open

n_2 number density of molecules along the electron beam - bypass closed

P_A pressure of gas in chamber A

P_B	pressure of gas in chamber B
S	pumping speed of the triode ion pump
t	unit of time
w	width of electron beam viewed by the spectrometer
y	distance of electron beam below the orifice between chambers A and B
	Temperatures
T_{T_i}	translation temperature of incident gas
T_{T_r}	translation temperature of reflected gas
T_{R_i}	rotational temperature of incident gas
T_{R_r}	rotational temperature of reflected gas
T_R	rotational temperature
T_s	surface temperature
$T_{spectrometer}$	rotational temperature measured by using the spectrometer
T_{true}	true rotational temperature
α_T	translation accommodation coefficient
α_R	rotional accommodation coefficient
α_i	internal accommodation coefficient
ϕ	function of rotational quantum number and temperature
μ	ratio of molecular weight of gas to the atomic weight of solid

ν	wave number
ν_o	wave number of rotational line (K',K'') = (3,2) in the (0,0) band of the first negative system
ρ	density of gas
ω	solid angle subtended by the orifice at a point P
Ω	constant defined in text
θ_D	Debye temperature of material of the solid
θ_o	angle noted on Figure 5
γ	ratio of specific heats

CHAPTER I

INTRODUCTION

At high temperatures and low densities, a gas in canonically distributed equilibrium follows the equipartition theorem. A diatomic gas in such an equilibrium has its internal energy divided between translational, rotational and vibrational degrees of motion in proportions which are kept in equilibrium by constant intermolecular collisions. This equilibrium can be disturbed in many ways. The passage of a shock wave, for example, would cause such a disturbance. From studies made on the passage of a shock wave through low density gases, it has been established that rotational and vibrational modes require many more collisions to come to equilibrium than the translational mode does.

Since energy exchange between a solid surface and a gas is also accomplished by collisions, it can be expected that the energy transfer to the internal modes is less than that to the translational mode. The accommodation coefficient provides a measure of the energy exchanged to each mode.

As the energy exchange between a solid surface and a gas obviously depends on the mechanism of surface atom-gas molecule interaction, many attempts have been made to predict theoretically, the results of such collisions. Thus, Maxwell, in extending to low pressure Poiseuille's law for capillary flow, suggested that a fraction f of the molecules colliding with a surface would be adsorbed and be diffusely reflected, while

(1-f) of the molecules would reflect specularly. Only the momentum history of the adsorbed molecules was considered. Nothing was said about their energies. M. Smoluchowski (1) used this idea and introduced a similar fraction f, which were adsorbed and reflected at the temperature of the surface. He showed this fraction f to be the same as the accommodation coefficient defined by Knudsen. Stickney's (2) experiments measuring normal momentum transfer of a molecular beam directed against a metal surface, led him to the conclusion that a fraction are fully accommodated and reflect diffusely with a velocity distribution corresponding to the surface temperature, while the remainder, experience no energy accommodation but are diffusely reflected. No special precautions were taken to remove adsorbed gas layers from the solid surface in these experiments and diffuse reflection can always be expected from gas covered surfaces.

A review of Knudsen's work can be found in Loeb's book (3) on the Kinetic Theory of Gases. The following account is derived from this source. Knudsen employed the kinetic theory of gases rather adroitly in his investigation of heat transfer at very low densities between two parallel plates separated by a distance less than the mean free path of the gas. He made the assumption that both the plates were "molecularly rough", meaning that gas molecules which collided with the plates left them at the temperature of the plates.

From kinetic theory, he obtained an expression for the energy transferred to the cooler plate as

$$E = \sqrt{\frac{2}{\pi}} \left[1 + \frac{3}{4}(k - 1)\right] \frac{P}{\rho_0} \frac{(T_1 - T_2)}{\sqrt{273T}} \qquad 1.1$$

where $k = \frac{2}{3(\gamma-1)}$, γ is the ratio of the specific heats c_p/c_v, T is the absolute temperature of the gas, and ρ_0 is the density in grams per cubic centimeter of the gas at 273°K and a pressure of one dyne per square centimeter. T_1 and T_2 are the temperatures of the plates and P is the pressure of the gas. Since E itself is difficult to measure because of radiation and residual gas conduction losses, measuring E at two pressures for a given $T_1 - T_2$ gives the ratio

$$\epsilon = \Delta E/\Delta P \Delta T \qquad 1.2$$

$$= 1819.2 \frac{\gamma+1}{\gamma-1} \frac{1}{\sqrt{MT}} \qquad 1.3$$

where M is the molecular weight of the gas.

Experimental results gave lower values for this quantity compared to those obtained from equation 1.3. At this juncture, Knudsen questioned the assumption of molecular roughness. He decided that the energy transfer between the gas and the surface was not complete as had been assumed. This led to the definition of accommodation coefficients. Knudsen defined the coefficient based on temperatures, which assumes Maxwellian equilibrium distribution at rest for the molecules. Much later, he conducted an experiment in which he obtained the translational accommodation by radiometric forces and

the total accommodation by the conduction of heat. In developing the theory for this experiment he assumed that the rotational energy of the molecules corresponded to that of a canonical energy distribution at the temperature of the solid surfaces. The results obtained for hydrogen and helium on a platinum strip, bright on one side and roughened on the other showed that the accommodation coefficients for the translational mode and for the internal mode were equal.

In modern literature, the coefficient of accommodation is defined as

$$\alpha = (E_i - E_r) / (E_i - E_s) \qquad 1.4$$

where E_i is the energy of the incident gas, E_r is the energy of the reflected gas, and E_s is the ideal energy if the gas is reflected at the temperature of the surface. This definition reduces to Knudsen's original definition of α based on temperatures, if both the incident and the reflected gas molecules have a Maxwellian velocity distribution.

In the present work, two accommodation coefficients have been used; the translational accommodation coefficient α_T, and the rotational accommodation coefficient α_R. These are defined as follows:

$$\alpha_T = (T_{T_r} - T_{T_i}) / (T_s - T_{T_i}) \qquad 1.5$$

where α_T is the translational accommodation coefficient, T_{T_r} is the translational temperature of the reflected gas molecules, T_{T_i} is the translational temperature of the incident molecules, and T_s is the temperature of the surface. Similarly,

$$\alpha_R = (T_{R_r} - T_{R_i}) / (T_s - T_{R_i}) \qquad 1.6$$

where T_{R_r} and T_{R_i} are the rotational temperatures of the reflected gas and the incident gas molecules respectively. Since the incident gas is in equilibrium, its translational and rotational temperatures are the same. The assumption that both incident and reflected gas molecules have Maxwellian energy or velocity distributions has been made in the above definitions, but since T_{R_r} is not necessarily equal to T_{T_r}, the reflected gas may not be in thermal equilibrium.

Although a considerable number of theoretical investigations of thermal accommodation of monatomic gases have been carried out (such as those in a series of papers by Goodman (4)), very little theoretical work has been put forward on accommodation of internal modes of energy of polyatomic gases. Even among the theories for thermal accommodation, a majority assume that the surface lattice is at 0°K and that the energy is given to it by the gas. This assumption makes these theories inapplicable as far as the present work is concerned. A few theories which do not assume a zero temperature solid are discussed below.

Logan and Stickney's (5) hardcube theory uses a simplistic model, proposed mainly to reduce the mathematical complexities of the more realistic models such as those of Goodman (4), and to take into consideration the thermal motion of the surface atoms. These are assumed to be hardcubes which have vibrational motion perpendicular to the surface. The interaction potential between these cubes and a gas molecule is a step function repulsive force which does not allow the gas molecule to spend any time on the surface. No trapping of the gas molecules is possible.

The results from such a model for molecular beams show one feature of interest: as the surface temperature increases the intensity maximum of the reflected molecule shifts towards the surface perpendicular, in agreement with experimental results cited by the authors.

Logan and Keck's (6) softcube theory is a logical extension of Logan and Stickney's (5) theory and assumes the potential between the solid cube oscillator and the gas molecule to be exponential. The theory was proposed mainly to provide better agreement with experimental results than the hardcube theory does. It also takes into consideration the trapping of gas molecules. The agreement given by the hardcube theory for the behaviour of the intensity maximum with temperature comes out of this theory also.

Among theoretical papers dealing with the internal mode of energies, those of Oman (7), Feuer (8) and Marsh (9) are of interest.

Oman has performed a computer simulation of the collisions between an incident gas of homonuclear molecules and a solid surface made up of atoms in a lattice. Again, the lattice has been taken to be at 0°K. The interaction potential is 6 - 12 Lennard-Jones type. The results show that the rotational energy exchange varies linearly with the translational energy of the incident molecules.

Feuer (8) has made a theoretical study based on a quantum mechanics model assuming a single phonon transition in the solid. The results indicate that the rotational accommodation coefficient is less than the translational accommodation coefficient. In a later paper, Feuer and Osburn (10) have calculated the two accommodation coefficients of para and ortho hydrogen on platinum at two temperatures, one above and one below the Debye temperature of the solid. Table 1. below shows their results and is reproduced from (10).

Table 1

Theoretical values of translational and internal accommodation coefficients

θ_D/T_s	T_s°K	α_T	$\alpha_i$para	$\alpha_i$para/$\alpha_i$ortho
2/3	338	0.337	0.0344	2.31
3/2	150	0.395	0.0423	7.30

The internal energy coefficient is very much less than the translational coefficient for both para and ortho hydrogen. The results given in Table 1. were obtained by considering only single phonon transition of the solid atoms. Two phonon transitions have been dealt with by Allen and Feuer (11) and they show that it contributes very little towards accommodation. For helium on platinum, for example, accommodation due to two phonon transitions is 1.33% of that due to single phonon transitions. Therefore the results considering only single phonon transitions should be good.

Marsh (9) has devised a gas-surface interaction model based on physical adsorption. Translational and internal energy accommodation coefficients are obtained from equations similar to gas-phase relaxation equations. The resulting expressions contain the relevant heats of adsorption. Results for diatomic gases, pertinent to this work, have not been obtained due to paucity of information about the heats of adsorption.

Experiments to determine thermal accommodation coefficient can be classified into two main categories: the first, in which the total thermal accommodation is obtained, and the second, in which both translational and internal coefficients are obtained.

Among the many methods belonging to the first category, Knudsen's low pressure method and the temperature jump method are perhaps the most popular. These methods are well known and have been documented

by various authors, including Wachman (12). Apart from the fact that these methods give only the total thermal accommodation, they are also limited in the temperature and composition of the solid surface that can be used.

Translational accommodation coefficient can be determined from molecular beam experiments. The method usually consists of shooting a monoenergetic beam of molecules at a given angle to the test surface, and then determining the number density and velocity of the reflected molecules at various angles with respect to the surface. Normal momentum accommodation is obtained from this. If the reflected molecules are assumed to have a Maxwellian velocity distribution, then the translational accommodation coefficient can also be determined. Accommodation of other modes is not determined by this method.

Of more interest and concern to the present work are the experiments belonging to the second category. Since there were no direct methods for measuring the internal energies until the electron beam fluorescence technique was developed, most of the experiments in the second category measured the internal energy accommodation by subtracting the translational accommodation from the total thermal accommodation.

Sasaki, Taku and Mitani (13) used a torsion balance to determine α_T. The test surface, in the form of a strip which can be electrically heated, is attached to one wing of the balance. A horizontal molecular

beam is shot at this strip. The translational coefficient is a function of the angles to which the balance rotates, depending on the temperature of the strip. The total thermal coefficient is obtained by measuring the heat loss from the strip when the strip is at the higher temperature (Knudsen's low pressure method). They obtained the values for $\alpha_T = 0.393$ and $\alpha_R = 0.314$ for a nickel strip at 518°C with nitrogen at 31.3°C.

In a later paper, Sasaki and Mitani (14) used a circular cross sectioned filament, shaped like an inverted V. They found the translational accommodation by relating it to the period of half decrement when the filament is set vibrating, with the translational motion of the molecules providing a damping mechanism to impede vibration of the filament. Again, the total thermal coefficient was found by Knudsen's low pressure method. They obtained $\alpha_T = 0.48$ and $\alpha_R = 0.10$ for tungsten at 300°C with hydrogen at 23°C.

Variations and modifications of the torsion balance method have been used by Stickney (2), Carpenter, Humphries and Nair (15) and many others, but mostly to obtain normal momentum coefficient or translational energy accommodation coefficient.

Schafer and Riggert (16) used a method claimed to be more accurate than that used by Eucken and Krome (17) to obtain both translational and internal energy accommodation coefficients. They heated a band of the test material in a Knudsen cell. A filament of the same

material fixed parallel to the band picked up heat from the reflected molecules. From this they were able to measure the thermal accommodation of the filament. They also determined the thermal accommodation coefficient of the filament alone by the low pressure Knudsen method.

Now, if all the modes of energy were equally accommodated, thermal accommodation found for the filament independently would be the same as that found when it is heated by the reflected molecules from the band. On the other hand, systematic differences in the two values can be related to partial accommodation coefficients.

Their results show that for nitrogen on gold, α_T decreases from .89 to .86 as T_s increases from 293°K to 389°K, and α_R decreases from .78 to .54 for the same temperature range.

A technique for direct measurement of rotational energy distribution of nitrogen molecules after reflection from a target surface was developed by Marsden (18), using electron beam excited fluorescence of light. Fluorescence from the beam at a point in front of the target was made up of contribution from molecules reflected directly from the target surface and from molecules of the background gas. The contribution from the background gas could be determined separately by retracting the target and this was then subtracted from the first measurement to obtain the contribution due to reflected molecules alone.

Results for a silver target showed that translational and rotational accommodation coefficients were equal and had a value of 0.85. It may be noted that the rotational energy distribution of the reflected molecules was found to correspond to that of a gas in thermal equilibrium. These results, were for a gas at higher temperatures than the surface.

The apparatus described in this thesis uses the electron beam fluorescence detector to provide simultaneous direct measurement of translational and rotational accommodation coefficients for nitrogen on a solid surface. It is an extension of the technique used by Marsden.

Two parameters were deemed to be of importance: the temperature of the surface T_s, and the ratio μ of the molecular weight of the gas to the atomic weight of the surface material. These parameters were varied during the experiment, keeping the incident gas nitrogen at room temperature. Measurements were made for a temperature range of T_s = 300°K to 900°K, and a μ range of 0.142 to 0.483.

CHAPTER II

EXPERIMENTAL APPARATUS

2.1 Vacuum System

The stainless steel vacuum system was constructed using inert gas welding technique for permanent joints and Varian Conflat type flanges with bakeable copper gaskets for demountable joints. An oven made of commercially available insulating material and covered with aluminum foil, enclosed the system and generated bakeout temperatures of about 300°C. A schematic of the system is shown in Figure 1. The different chambers have been labelled A, B and C to facilitate explanation. The top chamber A, is connected to chamber B by a 2.08mm. diameter orifice, as well as by a 37mm. diameter valved bypass. The bypass helps in reducing pressure in chamber A during bakeout. Chamber B sits atop chamber C and is separated from it by a large passage which presents virtually no obstruction to the flow of gas. The pressure in the two chambers are equal.

2.2 Chamber A

The gas-surface interaction takes place in chamber A. The gas introduction system on the left side of Figure 1 consists of a big plenum chamber from which gas is led into chamber A via a cold trap and two leak valves. A commercial gas bottle and a pump-stand are connected to the plenum chamber with the help of a tee-joint and

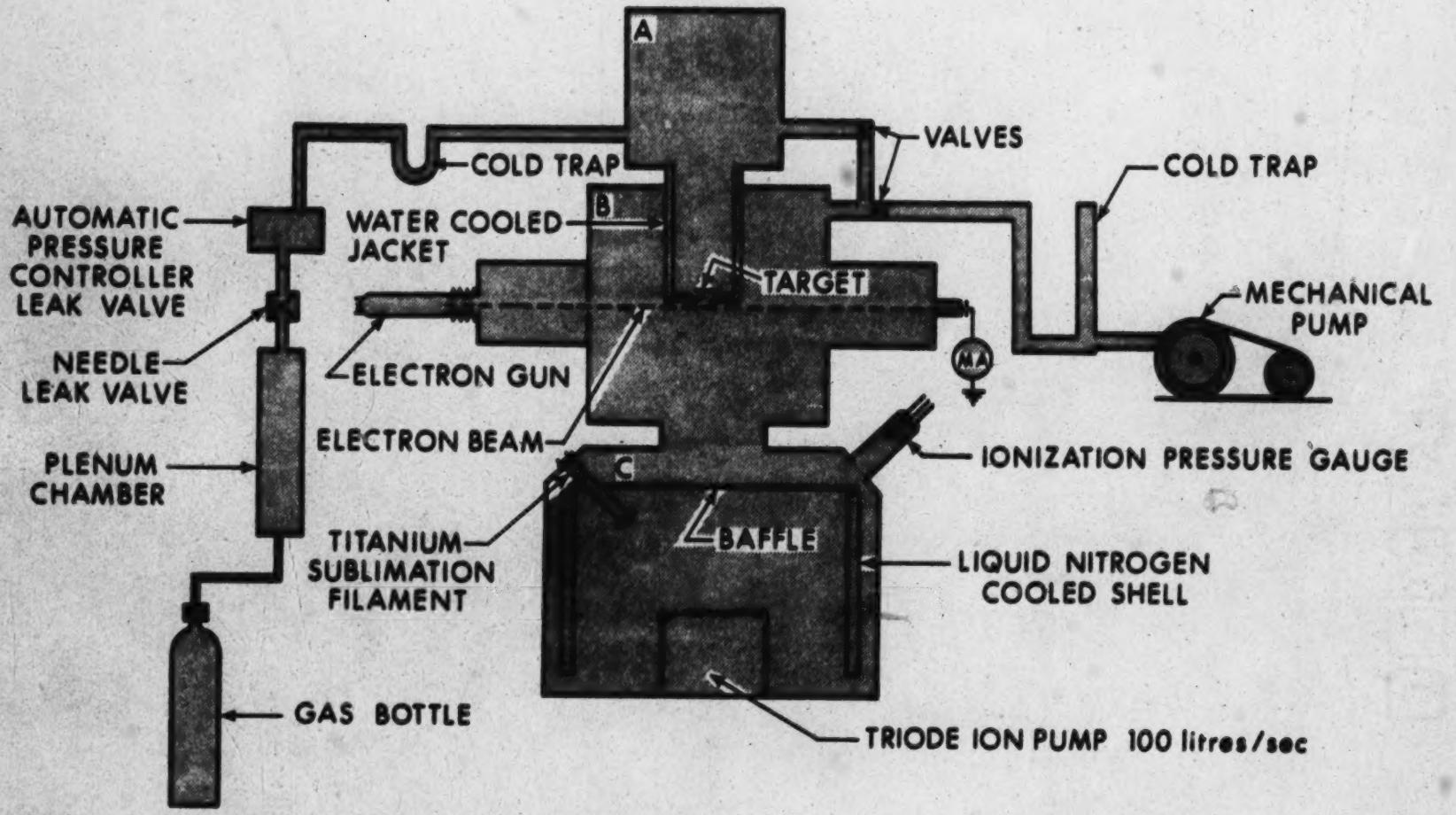

Figure 1. Schematic Diagram of the Experimental Apparatus.

appropriately located stop-cocks. The plenum chamber contains gas at high pressure and provides constant pressure upstream of the leak valves. The cold trap eliminates any moisture present in the gas and the leak valves are used to meter the flow of gas into the system. Chamber A is watercooled to keep the temperature of the gas constant.

The test surface is made of 0.005 or 0.01 inch thick, 7mm. wide sheet metal. Figure 2 shows the details. The target is U shaped lengthwise, the bottom flattened out to a plane surface about 10mm. long. The arms of the U are attached to the pinched ends of two heavy stainless steel tubes by screws and nuts. Both tubes are attached to the flange on top of chamber A, one of them being insulated from it. The location and other details and dimensions of the target are shown in Figure 2.

2.3 Chamber B

The roughing pump system is attached to chamber B on the right side in Figure 1. The pump system consists of a 4 litres per second rotary pump and a 100 litres per second oil diffusion pump. It is attached to chamber B by 37mm. stainless steel tubing. A cold trap is present in the connecting circuit. Rough pumping takes the vacuum system to about 1×10^{-5} torr pressure.

Chamber B also contains the electronbeam. A Phillips 902-564 television type electron gun to the left of chamber B produces a well

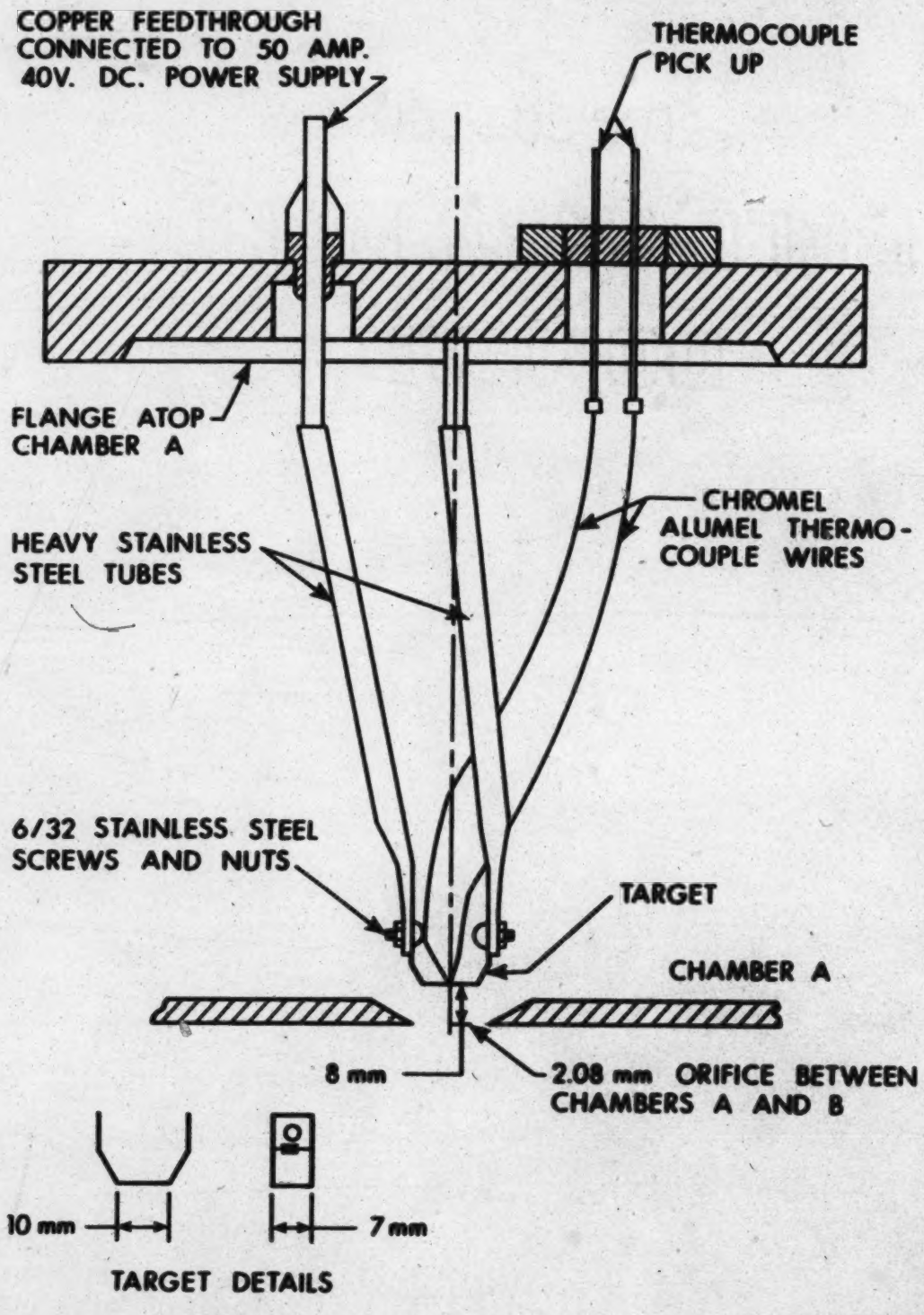

Figure 2. Target Mounting Details.

collimated, electrostatically focussed 1.5mm. diameter beam. The mechanism by which the gun is attached to chamber B facilitates adjustment of the location and direction of the beam. As shown in Figure 3, the beam passes through four 2.5mm. diameter holes, which locate it directly below the 2.08mm. orifice between chambers A and B. The power for the gun is supplied by an N.J.E. 0-30KV, 0-2.5ma. power supply. At normal operating filament current of 2.0ma and accelerating voltage of 10KV, about 1.1ma. beam current is obtained. This is picked up by the receiver on the right side of chamber B and is monitored by a digital milliammeter.

Some stratigically placed light baffles in chamber B prevent stray light from reaching the light sensing devices located outside a viewing port on chamber B.

2.4 Chamber C

Chamber C is the pumping chamber. It is large enough to prevent sudden fluctuations in pressure. A 100 litre per second triode ion pump and a titanium sublimation pump provide the pumping. To prevent heating of the gas by the sublimation pump, there is a liquid nitrogen cooled inner shell in chamber C. This shell also provides a cool surface upon which the subliming titanium molecules can settle. Only the ion pump was used while baking and for the final pump down. It provided a pressure of 7×10^{-9} torr. The sublimation pump was not

used during any part of the experiment as it proved incapable of providing constant pumping speed.

2.5 Pressure Measurement

A nude ultra high vacuum Varian ionization gauge attached to chamber C was used for the measurement of background pressure. As will be evident from the theory of this experiment, the background pressure needs only to be maintained constant. Since measurement of absolute pressure was not necessary, no accurate calibration of the ionization gauge was needed. The pumping current of the ion pump also provided a rough check on the total pressure.

2.6 Temperature Measurement

The target was heated ohmically by a 50 ampere 40 volt direct current power supply, connected to the copper feed through at the top of chamber A. A Chromel-Alumel thermocouple was spot welded to the target to measure its temperature. Calibration of the thermocouple was carried out outside the system and results were within $\pm$1°C of the values given in pertinent tables. The temperature gradient along the length of the target was also found by scanning with a radiation thermometer and it was ascertained that no cold spot was formed at the attachment point of the thermocouple.

The temperature of the test gas introduced into chamber A was assumed to be the same as that of the wall of chamber A. Two Chromel-

Alumel thermocouples attached to the wall measured the temperature. Any tendency for the wall to heat up due to radiated heat from the target and the leads was compensated for by adjusting the flow of cooling water. The walls were maintained at room temperature at all times.

2.7 Optics

The schematic of the optical system is shown in Figure 3. A cylindrical concave mirror, with its center of curvature coincident with the electron beam, reflects the fluorescent light to a 150mm. focal length double convex lens. The lens, which is outside the vacuum system in front of a viewing port in chamber B, focusses the image of the beam onto the entrance slit of the f/6 Czerny-Turner grating spectrometer. The spectrometer was placed on its side so that the slits were parallel to the beam. The intensity of the resolved spectrum lines was measured by an EMI 9502S photomultiplier.

The power for the photomultiplier was supplied by a Fluke model 410B 0-2.1 KV supply. It regulates output voltage within 0.001%. At normal operating conditions of -1.5 KV, the photomultiplier has a dark current of 4×10^{-10} amperes.

The output from the photomultiplier was measured by a Keithly 610 B Electrometer and recorded by a Honeywell Electronik 19 chart recorder.

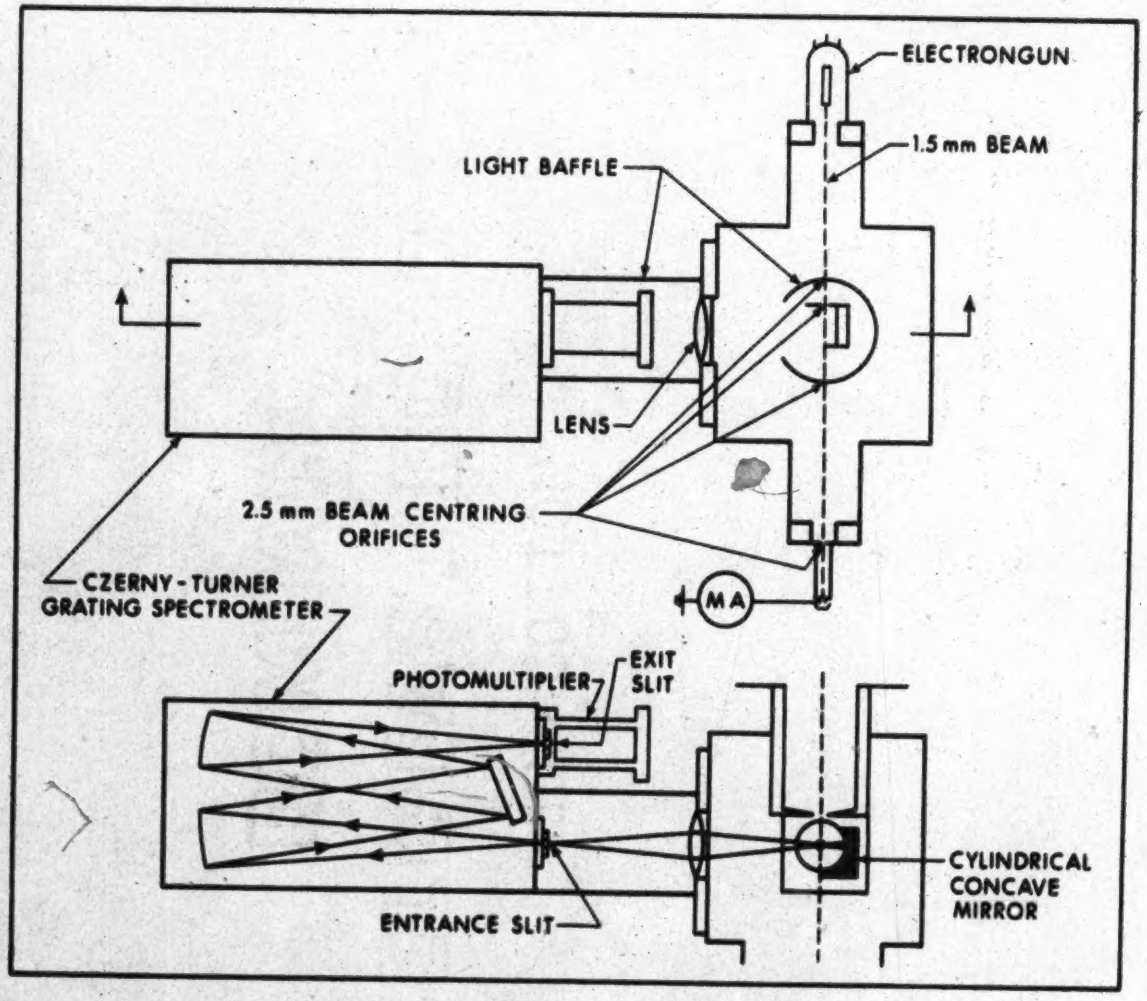

Figure 3. Schematic Diagram of the Optical System.

CHAPTER III

EXPERIMENTAL PROCEDURE

3.1 Surface Target Preparation

The target was cut out to the required size from 0.005 or 0.010 inch thick high purity metal foil. One face was cleaned with acetone and distilled water, and thermocouple wires were spot welded on it with a dial-a-weld telephone type welder. The target was then bent to shape and attached to the electrical leads as shown in Figure 2. Both the target and the leads were thoroughly cleaned with acetone and distilled water and dried with hot air. The whole assembly was then mounted onto chamber A, taking care not to leave greasy spots or fingerprints. The vacuum system was roughed, baked and pumped down to 7×10^{-9} torr pressure.

The target was heated to a high temperature (900°K in the case of nickel and gold, 750°K in the case of silver) at this pressure. Initially, the pressure went up to about 6×10^{-8} torr due to outgassing, but after an interval of about 2 hours, it settled down again to 7×10^{-9} torr, in which condition it was maintained for a period of twelve hours.

The stainless steel specimen was not cleaned in as thorough a fashion, since experiments on it were carried out while assessing the experimental method.

3.2 Introduction of Test Gas

The plenum chamber, the cold trap, and the manual leak valve were first pumped down to about 1×10^{-6} torr pressure. Nitrogen from the bottle was then introduced into them at about 5 psig. They were again pumped down. This process of flushing the system was carried out at least ten times to insure that the introduction system contained only nitrogen.

The plenum chamber was again filled with nitrogen to a pressure of about 5 psig. Every effort was made to keep this pressure constant by operating the bottle regulator whenever the gauges on the regulator showed a decrease. At this high upstream pressure of 5 psig, the servo driven needle valve failed to perform satisfactorily. It was therefore left open permanently. The manual needle leak valve was used to introduce gas into the main vacuum system and to control the background pressure.

Before any of the experiments were begun, a partial pressure gauge was attached to chamber C and the partial pressure of nitrogen at various total pressures was determined. Figure 4 is a graph of the results obtained. Tests were repeated a number of times and it was ascertained that the results shown on the graph did not vary.

After the target had been kept hot for 12 hours, the test gas was introduced into the system, and with the aid of the manual leak valve, the pressure as read by the ionization guage in chamber C was steadied to a constant value between 2×10^{-6} torr to 4×10^{-6} torr.

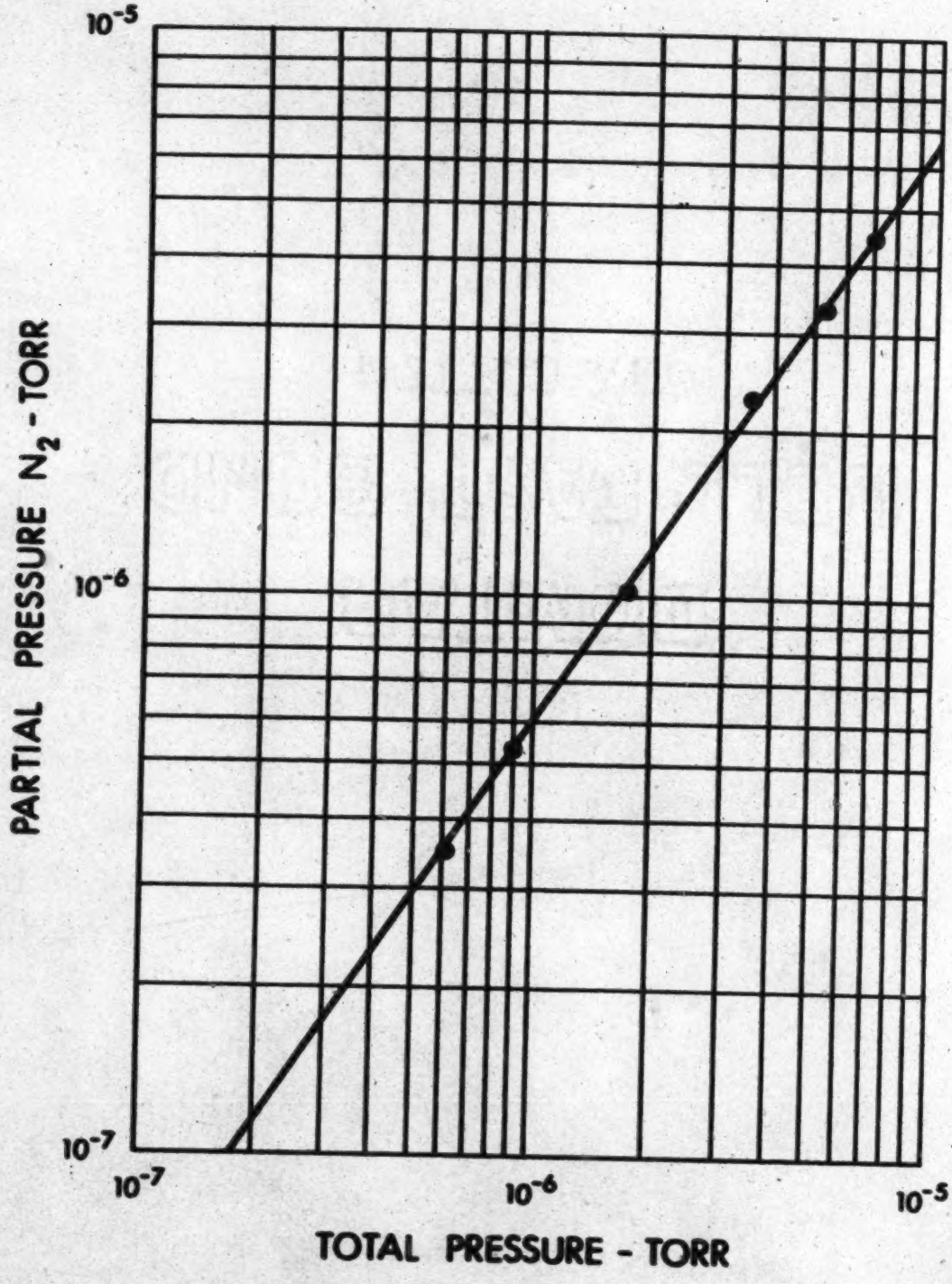

Figure 4. Partial Pressure of Nitrogen.

3.3 Determination of Accommodation Coefficients

After the target had been cleaned by heating, maintaining it at the same high temperature, the R branch of the $N_2^+(0,0)$ band emission was slowly scanned with the spectrometer. The results were recorded. Scans were carried out with the bypass valve between chambers A and B both open and closed. Measurements were made at a series of target temperatures varying from bake out temperature to room temperature in 100°K intervals.

The speed of scanning, the pressure measured by the ionization guage, the beam current, and the temperature of the incident gas were all kept constant during the entire duration of the experiment.

The experiment was repeated a number of times to test for repeatability.

CHAPTER IV

THEORY

4.1 Geometrical Considerations

A heated solid surface made up of the material to be tested is located in chamber A opposite a small orifice leading to chamber B as shown in Figure 1.

The pressure in chamber A is of the order of 10^{-4} torr, and the target surface is placed in such a way that substantially all the molecules reaching the electron beam from chamber A have come directly from the target surface with no intermediate collisions. The pressure in chamber B is kept as low as possible, typically 10^{-6} torr.

The valved by-pass connecting chambers A and B allows for pumping to outgas impurities that may be absorbed on the system walls. This by-pass is also used to reduce the pressure in A and thereby reduce the contribution of molecules coming through the orifice to a small fraction of the background density so that the contribution of the background gas in chamber B can be determined.

The number density of gas at a point P is $n = n_a + n_b$, where n_a is the contribution to number density by the molecules reflected from the target and issuing through the orifice, and n_b is the contribution of the background molecules in chamber B.

Since the gas in chamber A is in equilibrium and at rest, the velocity distribution is Maxwellian. It will be assumed that the reflected molecules come from a gas in equilibrium and at rest with a

temperature T_{T_r} and number density n_r, above the orifice. Consider a small area dA about point P subtending an angle dθ at centre of orifice, at an angle θ to the vertical, as shown in Figure 5.

The number of reflected molecules in solid angle dω passing through dA with a velocity c in time dt is:

$$N(c) = c^3 f_r \cos\theta \, dc\,dt\,d\omega\,dA/\cos\theta \qquad 4.1$$

Where dω is the solid angle subtended by the orifice at point P and f_r is the velocity distribution function of the reflected molecules. Now $d\omega = \frac{A'\cos^3\theta}{y^2}$ and $dA = \frac{y}{\cos\theta} wd\theta$, where w is the width of the beam which is observed through the slit of the spectometer, and A' is the orifice area.

The number passing through dA in time dt with velocity c is,

$$N(c) = c^3 f_r \frac{A'w}{y} \cos^2\theta d\theta\, dc\,dt \qquad 4.2$$

The number density of reflected molecules in dA is the number passing through dA divided by cdAdt,

$$\frac{N(c)}{cdAdt} = c^2 f_r \frac{A'}{y^2} \cos^3\theta\, dc \qquad 4.3$$

The number density due to reflected molecules of all velocities is obtained by integrating equation (4.3),

$$\int_0^\infty c^2 f_r \frac{A'}{y^2} \cos^3\theta\, dc = \frac{n_r}{4\pi} \frac{A'}{y^2} \cos^3\theta \qquad 4.4$$

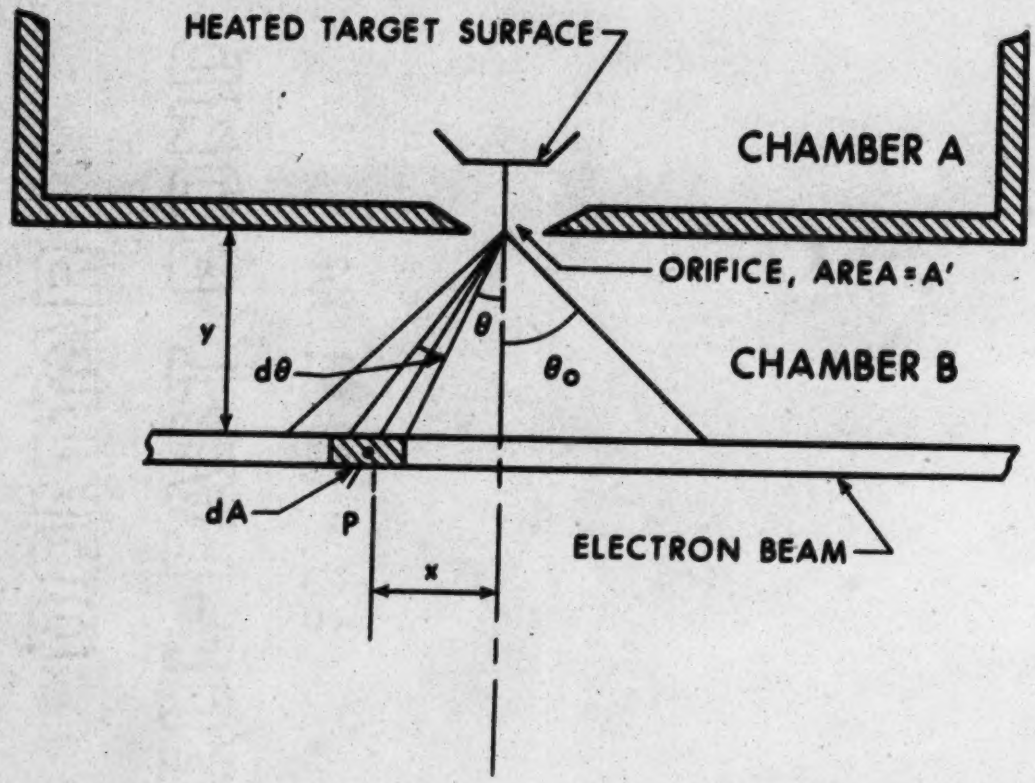

Figure 5. Details of the Detector Geometry.

The number density in dA due to background molecules is $n_B\ (1-\frac{d\omega}{4\pi})$.

The average number density in the length of beam viewed by the optical system is obtained by taking the integral

$$n = \frac{\int_{-\theta_0}^{\theta_0} \left| \frac{n_r}{4\pi} \frac{A'}{y^2} \cos^3\theta + n_B \left(1 - \frac{d\omega}{4\pi}\right) \right| dA}{\int_{-\theta_0}^{\theta_0} dA}$$

where $\pm\ \theta_0$ marks the ends of the portion of electron beam viewed.

$$n = \frac{(n_r - n_B)\ \frac{A'}{4\pi y^2} \left| \theta_0 + \frac{\sin 2\theta_0}{2} \right|}{\ln \frac{\tan \pi/4 + \theta_0/2}{\tan \pi/4 - \theta_0/2}} + n_B \qquad 4.5$$

This can be written as,

$$n = \Omega\ n_r + (1 - \Omega)\ n_B \qquad 4.6$$

The constant Ω depends only on system geometry.

When the bypass between A and B is closed, the orifice is the only connection between the two chambers. Let its conductance be C_1. Also let the speed of the triode ion pump be S, and the conductance of the bypass be C_2. Pressure in chamber A is related to that in chamber B by the relation $P_A = (\frac{S+C_1}{C_1})p_B$ when bypass is closed, and since the temperature in the two chambers is same, $n_A = (\frac{S+C_1}{C_1})n_B$. From conservation of mass at the target surface, $n_r = n_A \sqrt{T_1/T_r}$. Therefore,

substituting in (4.6)

$$n = \Omega\left(\frac{S+C_1}{C_1}\right)\sqrt{T_{T_i}/T_{T_r}}\, n_B + (1-\Omega)n_B \qquad 4.7$$

and similarly when the bypass is open,

$$n = \Omega\left(\frac{S+C_1+C_2}{C_1+C_2}\right)\sqrt{T_{T_i}/T_{T_r}}\, n_B + (1-\Omega)n_B \qquad 4.8$$

4.2 Electron Beam Measurements

The high energy electron beam excites and ionizes the neutral nitrogen molecules, which are initially in $N_2\ X^1\Sigma_g^+$ ground state, to an upper state $N_2^+ B^2\Sigma_u^+$. The light emitted comes almost entirely (19) from the first negative band due to the transition $N_2^+ B^2\Sigma_u^+ \rightarrow N_2^+\ X^2\Sigma_g^+$ of the nitrogen ion. If the doublets are not resolved, the transition becomes $^1\Sigma \rightarrow {}^1\Sigma$ and the applicable selection rule $\Delta K = \pm 1$, gives rise to two branches of emission P and R. The P branch has a vertex towards red on the Fortrat diagram and forms a bandhead. The R branch has peaks occurring at ever widening intervals towards the ultra-violet. A scan of the R branch of the $N_2^+(0,0)$ band is shown in Figure 6. The two to one alternation in intensity between odd and even numbered lines is a characteristic of nitrogen. The excitation emission mechanism is given in more detail in the Appendix.

The number density is determined by a summation of all the light output from one branch of the $N_2^+(0,0)$ band or alternatively by measuring the total light output from the unresolved band. Light intensity is given by the equation, $I = nk\phi$, where n is number density, k is constant

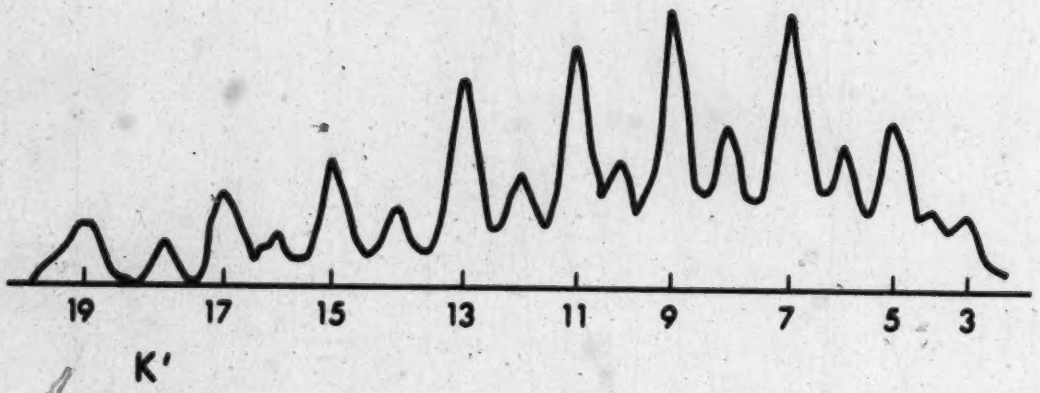

Figure 6. Spectrometer Scan of the R-Branch of the $N_2^+(0,0)$ band.

depending on the optical system and beam current and ϕ is a factor depending on the spectrum lines being observed. If the rotational spectrum is resolved $\phi(K',T_R)$ depends on rotational quantum number K' and rotational temperature T_R, n and k being constant. If the spectrum is unresolved and all light from the band is observed $I = nk\Phi$, where $\Phi = \sum_{K'=0}^{\infty} \phi(K',T_R)$. Φ is a constant, and I is then proportional to n.

The distribution of rotational energy, and the rotational temperature of the gas, can be obtained directly from a measurement of rotational line intensities (19). Rotational energy in a diatomic gas has the distribution (32) given by equation (4.9),

$$N_J = \frac{NhcB}{kT_R}(2J+1)e^{-Bhc\ J(J+1)/kT_R} \qquad 4.9$$

where N_J = number of molecules in rotational energy level J

N = total number of molecules

B = the rotational constant for the molecule

h = Planck's constant

k = Boltzmann's constant

c = speed of light

In the case of the $N_2^+(0,0)$ band of the nitrogen spectrum the line intensity distribution is given (19) by equation (4.10),

$$I(K') = (K' + K'' + 1)\chi_4[G]\frac{\nu^4}{\nu_0^4}e^{-BK'(K'+1)hc/kT_R} \qquad 4.10$$

where K is the rotational quantum number apart from spin ($J = K \pm 1/2$).

A single prime refers to the upper electronic state and double prime refers to the lower electronic state.

$$[G] = \frac{(K'+1)\exp[-2\,B\,(K'+1)\frac{hc}{kT_R}] + K'\,\exp[2B\,\frac{hc}{kT_R}\,K']}{(2K'+1)} \qquad 4.11$$

$[G]$ is a function of T_R,

χ_4 is a constant related to overall intensity, and

ν/ν_0 is approximately constant for a given band.

Equation (4.10) is derived from equation (4.9) by going through the process of excitation (and ionization) of the nitrogen molecules by the electron beam, followed by a spontaneous decay to the ground state of the ion with emission of light. The temperature T_R and rotational constant B appearing in both equations are the same.

A plot of $\mathrm{Log}[I(K')/(K'+K''+1)\,[G]\chi_4(\nu/\nu_0)^4]$ against $K'(K'+1)$ will result in a straight line with a slope $-Bhc/kT_R$ if the gas has a equilibrium rotational energy distribution.

Thus the rotational temperature T_R can be determined from a measurement of spectrum line intensities.

Figure 7 shows some plots of measured line intensities used to determine rotational temperature.

4.3 Translational Accommodation Coefficients

The translational energy accommodation coefficient, α_T, has been defined in equation 1.5 and can be written as,

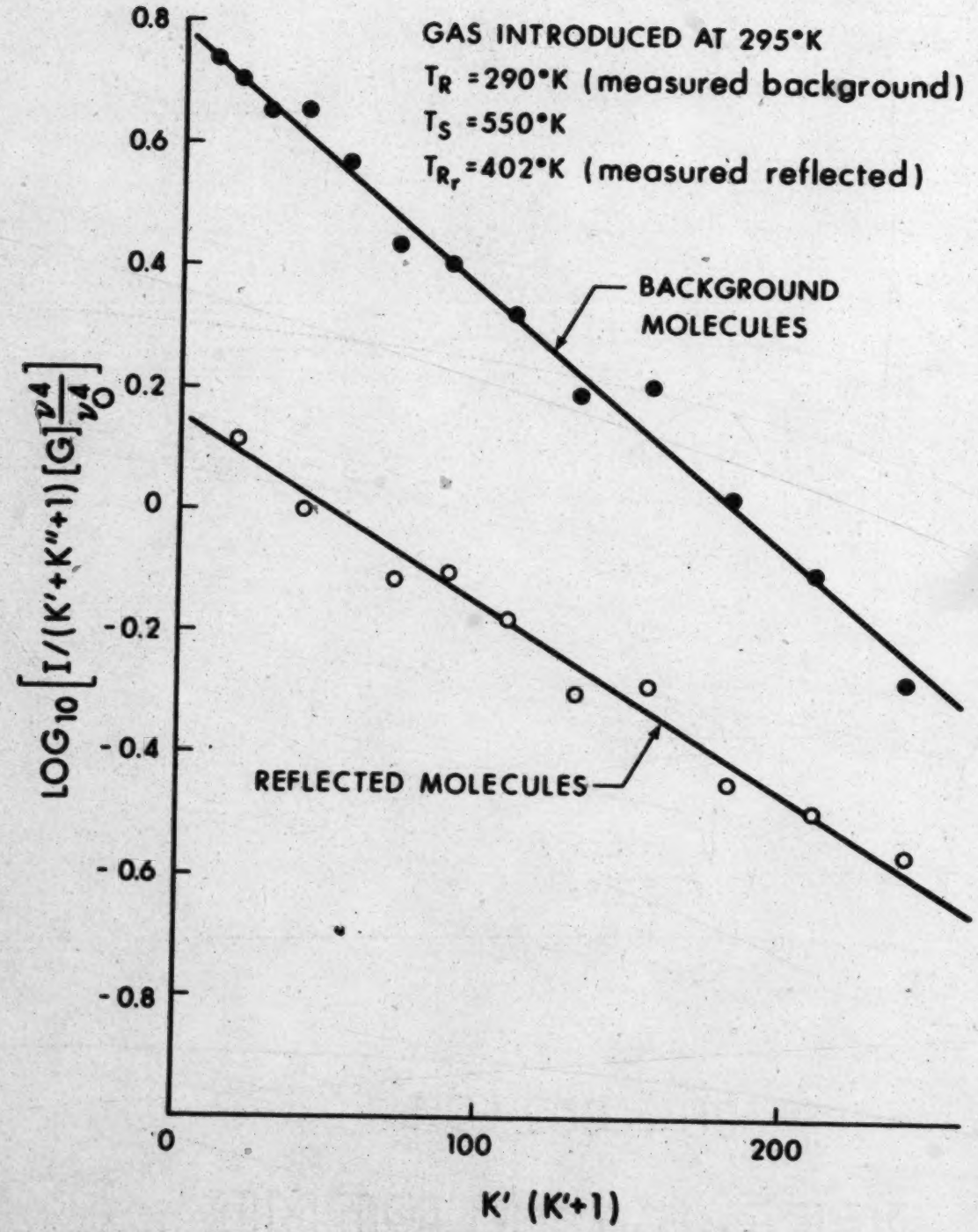

Figure 7. Typical Line Intensities in the Background and Reflected Molecules.

$$\alpha_T = (T_{T_r}/T_{T_i} - 1) / (T_s/T_{T_i} - 1) \qquad 4.12$$

where T_{T_i} is the temperature of the incident gas, T_{T_r} is the temperature of the reflected gas and T_s is the temperature of the solid surface. The temperature ratio T_{T_r}/T_{T_i} is determined experimentally as follows: When the bypass is open, the number density measured at the electron beam is,

$$n_1 = \Omega \left(\frac{S+C_1+C_2}{C_1+C_2}\right) n_B \sqrt{T_{T_i}/T_{T_r}} + (1-\Omega)n_B, \qquad 4.13$$

and when the bypass is closed the number density measured is,

$$n_2 = \Omega \left(\frac{S+C_1}{C_1}\right) n_B \sqrt{T_{T_i}/T_{T_r}} + (1-\Omega)n_B \qquad 4.14$$

Measurements were made with the target temperature the same as that of the incident gas ($T_s = T_{T_r} = T_{T_i}$), and at a higher temperature resulting in $T_{T_r} > T_{T_i}$. Then, for $T_{T_r} = T_{T_i}$,

$$(n_2-n_1)_{T_{T_i}} = \frac{\Omega S C_2}{C_1 (C_1+C_2)} n_B \qquad 4.15$$

and for $T_{T_r} > T_{T_i}$

$$(n_2-n_1)_{T_{T_r}} = \frac{\Omega S C_2}{C_1 (C_1+C_2)} n_B \sqrt{T_{T_i}/T_{T_r}} \qquad 4.16$$

Therefore

$$\frac{(n_2-n_1)_{T_{T_r}}}{(n_2-n_1)_{T_{T_i}}} = \sqrt{T_{T_i}/T_{T_r}} \qquad 4.17$$

Since $I = kn\phi$ and since k and ϕ are constants,

$$\frac{\sqrt{T_{T_r}}}{T_{T_i}} = \frac{(I_2 - I_1)_{T_{T_r}}}{(I_2 - I_1)_{T_{T_i}}}$$

where $I = \sum_{K'=1}^{17} I(K')$, and subscripts 1 and 2 refer to the bypass open or closed respectively.

From equation (4.12)

$$\alpha_T = \frac{[(I_2-I_1)_{T_{T_i}}/(I_2-I_1)_{T_{T_r}}]^2 - 1}{T_s/T_{T_i} - 1} \qquad 4.18$$

4.4 Rotational Accommodation Coefficient

Line intensities of the R-branch of $N_2(0,0)$ band for the molecules reflected from a heated surface are obtained in this experiment by subtracting the line intensities scanned with the bypass valve between chambers A and B open from those when it is closed. The rotational temperature of the reflected molecules is determined from these measured line intensities.

The number density n from equation 4.6 is

$$n = \Omega n_r + (1 - \Omega)n_B$$

The intensity of a measured spectrum line corresponding to rotational level K' can be written as

$$I(K') = \Omega n_r\, k\phi(K', T_{R_r}) + (1 - \Omega)n_B\, k\phi(K', T_{R_i}) \qquad 4.19$$

where, as before, k depends on the geometry of the optical system and

ϕ is a function of K' and the temperature of the gas.

Equation 4.19 can be written as

$$I(K') = \Omega I_R(K', T_{Rr}) + (1-\Omega)\, I_B(K', T_{R_i}) \qquad 4.20$$

where $I_R(K', T_{R_r})$ is the contribution to line intensity at K' of the reflected gas molecules at a rotational temperature T_{R_r}, and $I_B(K' T_{R_i})$ is the contribution of the background molecules at temperature T_{R_i}.

As indicated before, the R-branch is scanned with the bypass valve open and closed, keeping all the other variables constant. The gas number densities in the two cases are examined below.

When the bypass valve is open, the number density n is given by equation 4.8. Substituting S = 100 liters per second, C_2 = 20 liters per second, C_1 = 0.4 liters per second and Ω = 0.001876 (obtained by substituting appropriate values in equation 4.5), equation 4.8 becomes

$$n = 0.011072\, n_B \sqrt{\frac{T_{T_i}}{T_{T_r}}} + 0.998124\, n_B \qquad 4.21$$

where the first part of the right hand side of the equation is the contribution of the reflected molecules at a translational temperature T_{T_r}, and the second part is the contribution of the background molecules.

In the present experiments, T_{T_r} was always greater than or equal to T_{T_i} because the surface target temperature was always greater than or equal to the temperature of the incident gas. In view of this, the maximum value of $\sqrt{T_{T_i}/T_{T_r}}$ is 1.0.

Equation 4.21 reduces to

$$n = 0.011072\, n_B + 0.998124\, n_B \qquad 4.22$$

which reveals that the contribution of the reflected molecules to the total number density is about 1% while the background molecules contribute 99%.

At this juncture an approximation will be made that

$$n = n_B \qquad 4.23$$

when the bypass valve is open. This approximation will be eliminated by a refining process, shown later.

With this approximation equation 4.20 reduces to

$$I(K') = I_B(K', T_{R_1}) \qquad 4.24$$

when the bypass valve is open.

Since these line intensities are from background gas molecules known to be at 295°K, instead of taking I(K') directly from the spectrographic scan, the corresponding theoretical values are taken to eliminate unnecessary scatter in the results.

The slope of the line used to determine the rotational temperature is Bhc/kT_R, and for $T_{R_1} = 295°K$ has a value of 0.004237 on the common log scale.

Using the negative of this slope, an equation for a straight line is written as $y = -0.004237\ x+C$

where $y = \log I(K')/[(K'+K''+1)[G](\frac{\nu}{\nu_0})^4]$ and $x = K'(K'+1)$.

C is an arbitrary constant, and for the present can be taken as 0.

From this equation x and y are calculated for various values of K'. The calculated values are given in Table 2. For even values of K', I(K') has half the value given by the equation as explained in the appendix.

Table 2

Theoretical values of line intensities at room temperature

K'	x	y	$\log (K'+K''+1)[G](\frac{\nu}{\nu_0})^4$	I(K')
3	12	-.0508	.7712	5.252
4	20	-.0847	.8971	3.246
5	30	-.1271	.995	7.377
6	42	-.178	1.0752	3.946
7	56	-.2373	1.1431	8.051
8	72	-.3051	1.2031	3.954
9	90	-.3813	1.2563	7.499
10	110	-.4661	1.3045	3.447
11	132	-.5593	1.3484	6.153
12	156	-.6609	1.3882	2.668
13	182	-.7711	1.425	4.507
14	210	-.8898	1.4602	1.859
15	240	-1.0169	1.4937	2.994

In column 4 of Table 2, [G] is calculated from equation 4.11 and values

of ν are taken from Child's (20) paper. To distinguish calculated values from measured values of intensities, let the values given in Table 2 be called $I_{table}(K')$.

Values of $I_{table}(K')$ from K' = 3 to 15 are summed up. This sum is equal to 60.9535. Values of I(K') from the experimental scan of the R-branch with the bypass valve open are also added to obtain $\sum_{K'=3}^{15} I(K')$. In the first approximation, $I_B(K')$ is taken to be

$$I_B(K') = \sum_{K'=3}^{15} I(K') \times I_{table}(K')/60.9535 \qquad 4.25$$

Now, when the bypass valve is closed, the number density n is given by equation 4.7.

Substituting values for S, C_1, and Ω,

$$n = 0.470 n_B \sqrt{T_{T_i}/T_{T_r}} + 0.998124 n_B \qquad 4.26$$

where, again, the first part of the right hand side is the contribution of the reflected gas molecules, and the other part is that of the background gas molecules. In the present experiments, the maximum value that T_{T_r} reached was 537°K corresponding to $\alpha_T = 0.4$ at $T_s = 900$°K for gold. This gives $\sqrt{T_{T_i}/T_{T_r}} = 0.7425$. Equation 4.26 becomes

$$n = 0.3496 n_B + 0.998124 n_B \qquad 4.27$$

It is of interest to note here that the contribution of the reflected molecules to the total number density varies between $0.3496 n_B$ and $0.4708 n_B$ corresponding to $T_{T_r} = 537$°K and $T_{T_r} = 295$°K.

Examining equations 4.26 and 4.20, values of the line intensities, $I_R(K')$, due to the reflected molecules, can be obtained by subtracting $I_B(K')$ (given by equation 4.25) from the line intensities obtained by scanning the R-branch with the valve closed. The result can be written as

$$\Omega I_R(K') = I(K') - I_B(K') \qquad 4.28$$

A computer program was written to fit a least squares line to points given by plotting $\log \Omega I_R(K')/(K'+K''+1)[G](\frac{\nu}{\nu_o})^4$ against $K'(K'+1)$.

This program is given in the appendix. From the negative of the slope of this line, the rotational temperature of the reflected gas molecules T_{R_r} is obtained.

As was noted, an approximation was made in writing equations 4.23 and 4.24. The value of T_{R_r} found above contains this approximation. A refining procedure to correct this follows.

Substituting the value of the translational temperature T_{T_r} in equation 4.21, the total light contribution of the reflected gas molecules can be written as

$$\sum_3^{15} I_R(K') = \frac{\sum_3^{15} I(K')}{0.011072 \sqrt{\frac{1}{T_r}} + 0.998124} \times 0.011072 \sqrt{T_{T_i}/T_{T_r}} \qquad 4.29$$

and

$$\sum_3^{15} I_B(K') = \sum_3^{15} I(K') - \sum_3^{15} I_R(K') \qquad 4.30$$

Values of $\Sigma I_B(K')$ given by equation 4.30 are used to find the corresponding theoretical line intensities as was done in Table 2. These theoretical values are substituted into equation 4.28 to obtain $I_R(K')$ and subsequently the rotational temperature T_{R_r} from the computer program.

In practice, however, it was found that the approximate equation 4.24 for $I_B(K')$, corrected as per Table 2, resulted in values of T_{R_r} which were within 0.06% of the value found after refining.

Once the rotational temperature T_{R_r} is found, the rotational accommodation coefficient is given by equation 1.6

$$\alpha_R = (T_{R_r} - T_{R_i}) / (T_s - T_{R_i}) \qquad 1.6$$

The pumping speed S and the value of the conductance C_2 are known only approximately, but this does not affect the accuracy very much. In equation 4.21, if the value of S is taken to be 50 liters per second instead of 100 liters per second

$$n = 0.00776 n_B \sqrt{T_{T_i}/T_{T_r}} + 0.998124 n_B \quad \text{and}$$

if T_{T_i}/T_{T_r} is taken to be unity as was done to obtain equation 4.22, then

$$n = 0.00776 n_B + 0.998124 n_B$$

which, when compared to equation 4.22, gives better justification to the assumption made in writing $n = n_B$. It is doubtful that the value of S would exceed the 100 liters per second specified by the manufacturers.

Similarly, C_2 has been assumed to be 20 liters per second based on the geometrical dimensions of the 37 mm. inch tubing bypass connecting chambers A and B. Substituting two values which differ by ten liters per second from the value assumed for C_2 in equation 4.8,

$$n = 0.01991n_B + 0.998124n_B$$

for C_2 = 10 liters per second if T_{T_i}/T_{T_r} is unity, and

$$n = 0.008047n_B + 0.998124n_B$$

for C_2 = 30 liters per second.

Comparison of these two equations to 4.22, which has C_2 = 20 liters per second, indicates that the contribution of the reflected molecules (the first part of the right hand side) is altered by less than 1%.

Thus, the values of S and C_2, which are known only approximately, do not affect the accuracy of the method very much.

CHAPTER V

RESULTS AND DISCUSSION

5.1 Rotational Accommodation Coefficient

Figure 8 shows the variation of rotational accommodation coefficient α_R with target surface temperature T_s for nickel, silver and gold. The value of α_R is about 0.15 for nickel and gold. There appears to be very little variation with T_s. For silver, however, α_R varies from 0.03 at 400°K to 0.2 at 700°K.

Results of Sasaki, Taku and Mitani (13) show that at T_s = 791°K and T_{R_1} = 304.3°K, α_R = 0.314 for nickel and nitrogen. Results obtained in the present work for the same temperature and surface give α_R = 0.17, which is about half in magnitude. The difference is probably due to the condition of the test surfaces. It is well known that accommodation coefficients are sensitive to surface condition. For example, it was noticed during the present experiments that stainless steel, which will have an oxide covered surface, exhibited high values of α_R (Figure 9). Sasaki, Taku and Mitani (13) have not given enough information in their paper to draw any conclusions about the condition or their solid surface or the reliability of their measurements. No attempt appears to have been made to clean the surface, other than working at high temperatures. Sasaki and Mitani (14) in a later paper give α_R = 0.10 for hydrogen and tungsten at T_s = 573°K and T_{R_1} = 296°K. This value seems more in keeping with the values measured in the present experiment for both nickel and gold with nitrogen.

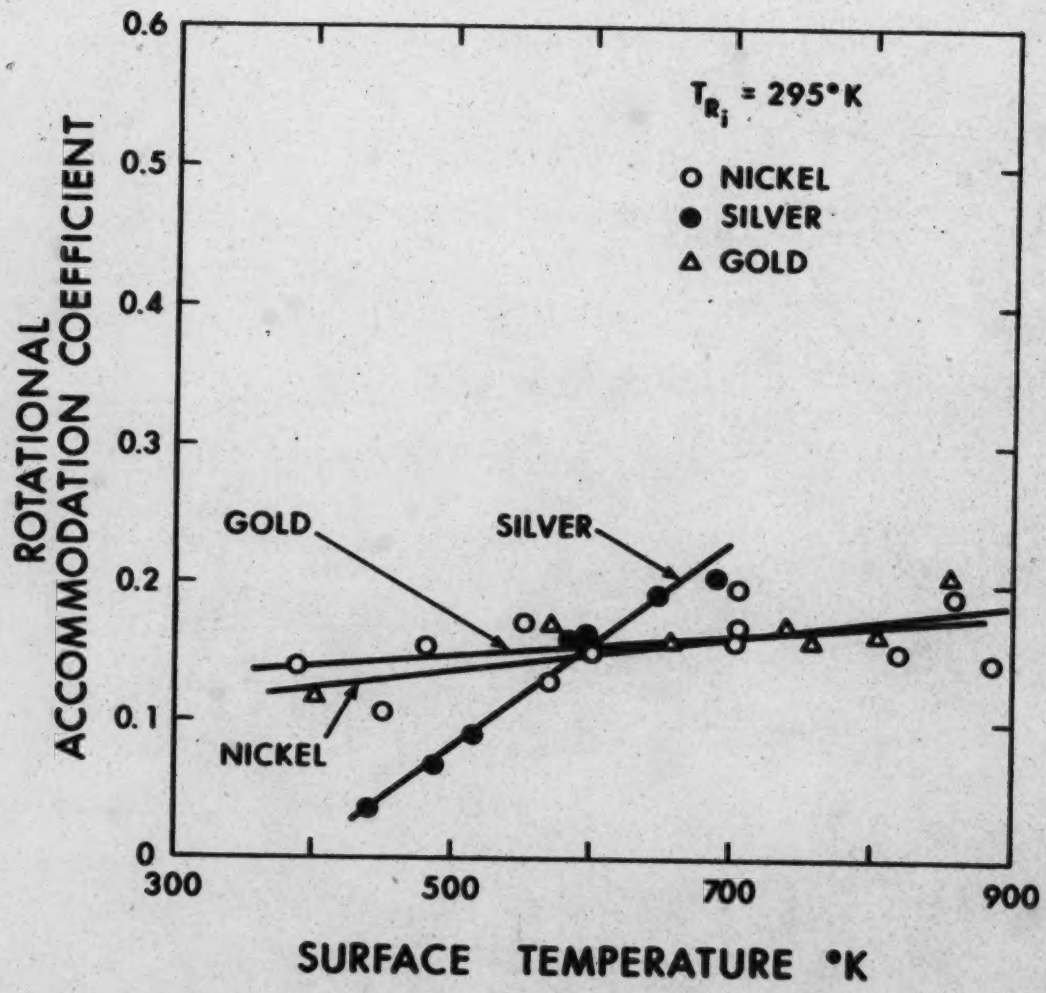

Figure 8. Variation of Rotational Accommodation Coefficient of Nickel, Silver and Gold with Surface Temperature.

The results of Schafer and Riggert (16) show that for gold and nitrogen α_R reduces from 0.78 to 0.54 as T_s increases from 293°K to 389°K. In the two methods they employ for determining the accommodation by the filament, the filament is heated by hot gas reflecting from a heated band in one case, and in the other it is ohmically heated. Thus, in the former case, energy is being given by the gas to the solid, while in the latter, the heated solid gives energy to a colder gas. Both Sasaki et al and Schafer and Riggert have used indirect methods to deduce α_R. The accuracy of such methods is hard to assess.

Results of both Knudsen (21) and Marsden (18) show that the rotational and translational accommodation coefficients are equal. Knudsen found that the difference in both translational and thermal coefficients for rough and smooth surfaces was equal for monatomic and diatomic gas. Marsden obtained $\alpha_R = 0.85$ for nitrogen on silver. It should be noted that this result was obtained with the gas heated and the surface cold in contrast to the results obtained from room temperature gas and hot surfaces in the present experiment.

The amount of theoretical work that has been done for predicting rotational accommodation coefficients is very limited. Feuer's (8) theory, based on a quantum mechanical model, states that α_R should be less than α_T. This has been found to be generally true in the present work.

Oman's (7) theory, based on computer simulation of the collision

process, states that the energy exchange to the rotational mode is linearly proportional to the energy in the translational mode of the incident gas. The theory is based on a solid assumed to be a lattice of discreet atoms at 0°K. It has not been possible to check this theory because the translation energy of the incident gas was constant and the surface was at a higher temperature in the present experiments.

An analysis of the expected accuracy of the present experiments is given below, following which some aspects of the method used for determining the rotational temperature of the gas are discussed.

5.2 Estimation of Accuracy of Measured Rotational Accommodation Coefficient

Rotational accommodation coefficient α_R is given by equation 1.6:

$$\alpha_R = (T_{R_r} - T_{R_i}) / (T_s - T_{R_i}) \qquad 1.6$$

Both T_{R_i} and T_s were measured by calibrated thermocouples. The error is not expected to be more than ± 1°K. Experiments conducted with $T_s = T_{R_i} = 295$°K (room temperature) showed that the scatter of experimental points from a least squares best fit line had a standard deviation of 3.2% corresponding to extreme values of rotational temperature T_{R_r} of $T_{R_r} \pm 9$°K. The slope of the least squares fit line gave the values of T_{R_r} to be 295°K ± 5°K. The results of a typical run are shown in the appendix. The calculated value of T_{R_r} was found to be 290°K for this data.

At higher target temperatures, T_{R_r}, measured by subtracting two

sets of line intensities, one of which is 1.5 times the other, shows considerably more scatter. The computer program given in the appendix prints out the rotational temperature after points lying more than a standard deviation away from the least squares fit line are removed. It also prints out the extreme rotational temperatures corresponding to the variation in slope due to standard deviation. The results gave a scatter in the rotational temperatures of less than $\pm 4\%$.

Since the scatter and the line intensities are independent of temperature and the slope of the best fit line is proportional to $1/T_{R_r}$, the error in T_{R_r}, namely ΔT_{R_r}, will be proportional to T_{R_r}. Hence, the scatter will cause ΔT_{R_r} to be $\pm 0.04 T_{R_r}$.

The rotational accommodation coefficient can be written as

$$\alpha_R = (T_{R_r} \pm \Delta T_{R_r} - T_{R_i})/(T_s - T_{R_i}) = \alpha_R \pm 0.04 \left| \alpha_R + \frac{T_{R_i}}{T_s - T_{R_i}} \right| \qquad 5.1$$

The limits of error given by this expression have been plotted on Figure 9 which shows the results for stainless steel. It is evident that the possible error increases beyond 10% for T_s below 440°K. The error decreases as T_s increases and α_R decreases.

It seems appropriate at this stage to examine the accuracy of the method used for determining the rotational temperature. The method was developed by Muntz (19). Its accuracy has been questioned by Ashkenas (22) and Harbour (23) among others.

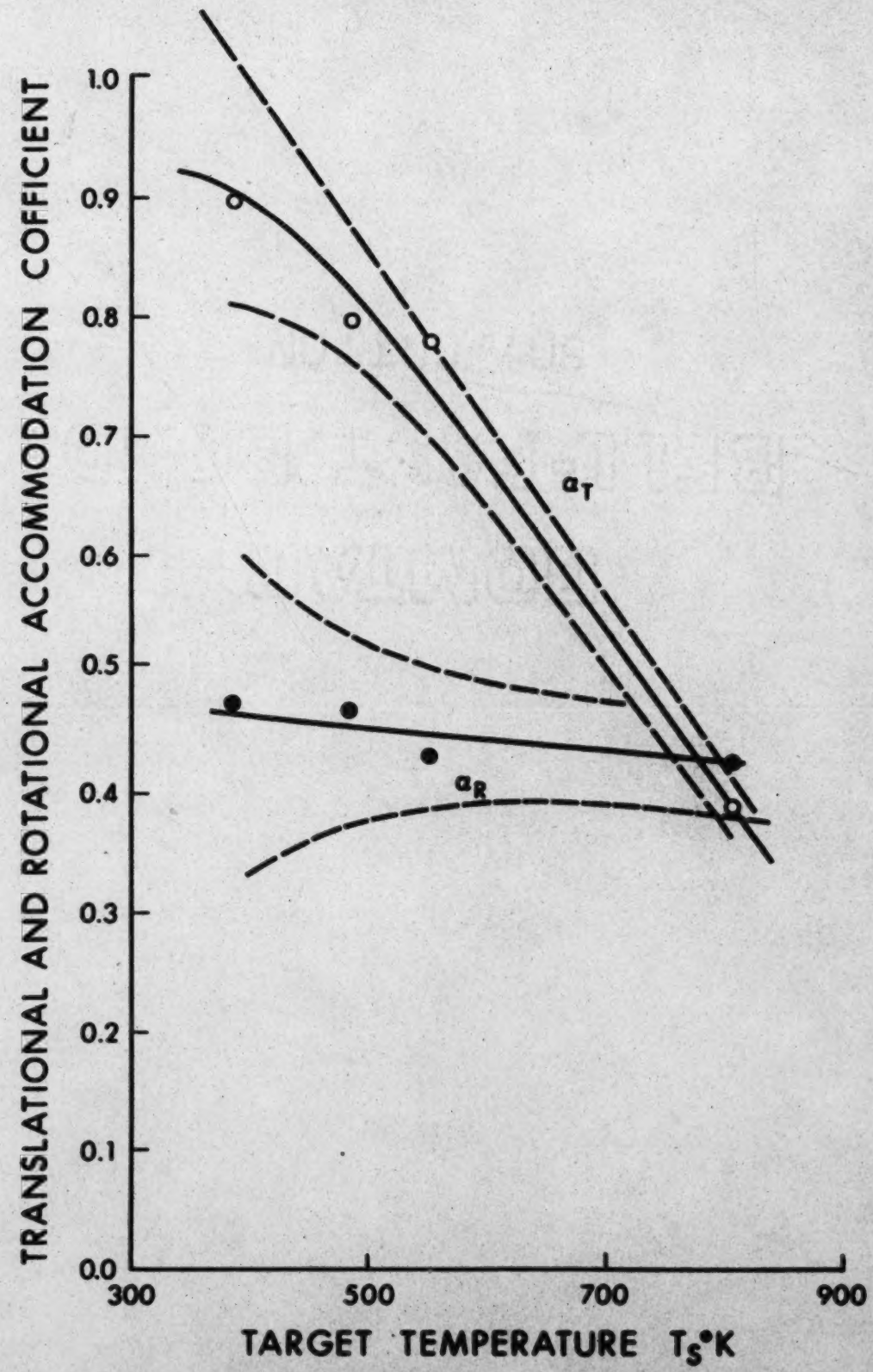

Figure 9. Variation of Theoretical Error Limits of Accommodation Coefficients of Stainless Steel with Surface Temperature.

Experiments by Marsden (18), Robben and Talbot (24) and Ashkenas (22) indicate that the measured rotational temperature is too high. The error increases with increase in density of the gas and decrease in its temperature. Ashkenas further suggests that the temperature depends on the number of peaks considered.

Ashkenas concludes that above T_R = 300°K, the rotational temperature can be measured with less than 10°K error without applying corrections he has suggested for density, temperature and the number of peaks. Based on a number of results, a statistically corrected equation of the form

$$T_{spectrometer}/T_{true} = A + B \log\rho \qquad 5.2$$

has been developed. The values of A and B are given in Figure 10 of his paper. At 300°K, for the number of peaks (10 to 13) and density (7×10^{-8} gms per cubic cm.) used in the present work, A = 1.36 and B = 0.05. The equation 5.2 then becomes

$$T_{spectrometer}/T_{true} = 1.36 + 0.05 \log 7 \times 10^{-8}$$
$$= 1.002255 \qquad 5.3$$

This shows that at 300°K, which is the lowest gas temperature used in the present experiments, the error is about 0.2%. For higher temperatures, the error is expected to be less than this.

The discrepancy in rotational temperature has been attributed to secondary electrons produced, which do not necessarily follow the optical selection rule $\Delta K = \pm 1$.

Lillicrap (25) has proposed a theory in which the secondary electrons are taken into consideration by altering the equation put forth by Muntz (equation 17 of (19)) to

$$I(K')/2K'(G_p + nG_s) \text{ proportional to } \exp\left|- K'(K'+1)/T_R\right| \qquad 5.4$$

where G_p is the same as [G] in Muntz' equation for primary electrons, G_s is similar to G_p, for secondary electrons, and n is the number density of the gas. The above equation reduces to that of Muntz as $n \to 0$. Experimental data cited by Ashkenas (22) confirms the veracity of equation 5.4.

Lillicrap has plotted a graph of line intensities normalized by dividing them by the highest line intensity, (I(3) at 80°K) against density. The plot shows that the use of his method gives good agreement for all densities. It also shows that equation given by Muntz produces good results below 1×10^{16} molecules per cubic centimeter. The present experiments were conducted with a number density of 1.54×10^{15} molecules per cubic centimeter.

Harbour (23) contends that there is a possibility of very high concentration of the secondary electrons. Experimental results of Dunn and Self (26) in parallel geometry collisionless flow are cited. It should be noted that their experimental set up was dissimilar to the one used during the present experiments. Mean energy of the secondaries is taken as 20 eV and the most probable energy as 0.6 eV. The secondaries are assumed to reach equilibrium temperature of 2 eV quickly. Harbour

argues that the electrostatic field of the ions reduces the radial velocity of the secondaries, and the field of the secondaries increases the radial velocity of the ions. This argument does not apply to the present experimental set up as the primary beam is not confined and there is no reason for ions to congregate near the beam centre. The field of the primary should stay negative. The extent to which Harbour's argument holds may be the reason the results improve at higher temperatures. In a geometry like the one presently used, the ions which inhibit the radial velocity of the secondaries should move out of the region of interest more quickly at higher temperatures because their own velocity would be very near that of the thermal agitation velocity of the gas molecules.

Since the density in the present case is very much lower than those used in the experiments by most of the others mentioned, and the temperature equal to and above 300°K, the measured rotational temperatures are expected to be within the $0.04T_R$ scatter predicted by the analysis of experimental errors.

5.3 Translational Accommodation Coefficient

Figure 10 shows the variation of translational accommodation coefficient α_T with target surface temperature T_s, for nickel, silver and gold. The translational accommodation coefficients are 0.5, 0.4 and 0.2 at 400°K respectively for nickel, silver and gold. The variation of α_T with T_s approximates to the equation

$$d\alpha_T/dT_s = -13.7278 \times 10^{-4} + 2.6042 \times 10^{-4}/\mu \qquad 5.5$$

where μ is the ratio of the molecular mass of nitrogen to the atomic mass of the material of the surface.

Among the works cited before, the results of Sasaki, Taku and Mitani (13) show that at $T_s = 791°K$ and $T_{T_1} = 304.3°K$, $\alpha_T = 0.393$ for nickel and nitrogen. Present results give $\alpha_T = 0.18$ for the same conditions. The difference can probably be attributed to the difference in the condition of the test surfaces in the two experiments. Sasaki, Taku and Mitani calculated α_T from the rotation of the torsion balance when a beam of molecules impinged on the test surface. The method used by Stickney (2), consisting of rotating of the balance shaft to keep the test surface in the same position, appears to be a better method of conducting this type of experiment.

Sasaki and Mitani (14) have given the value of $\alpha_T = 0.48$ for hydrogen on tungsten at 573°K. Neither of the above mentioned works give the variation of α_T with T_s.

Results of Schafer and Riggert (16) for gold and nitrogen show that α_T decreases from 0.89 to 0.86 as T_s increases from 293°K to 389°K. The values appear rather high.

Marsden (18) has given $\alpha_T = 0.85$ for silver and nitrogen, but his values are for a heated gas on a cold surface.

The more interesting result of the present study is the behaviour of α_T with changes in surface temperature. There appears to be a

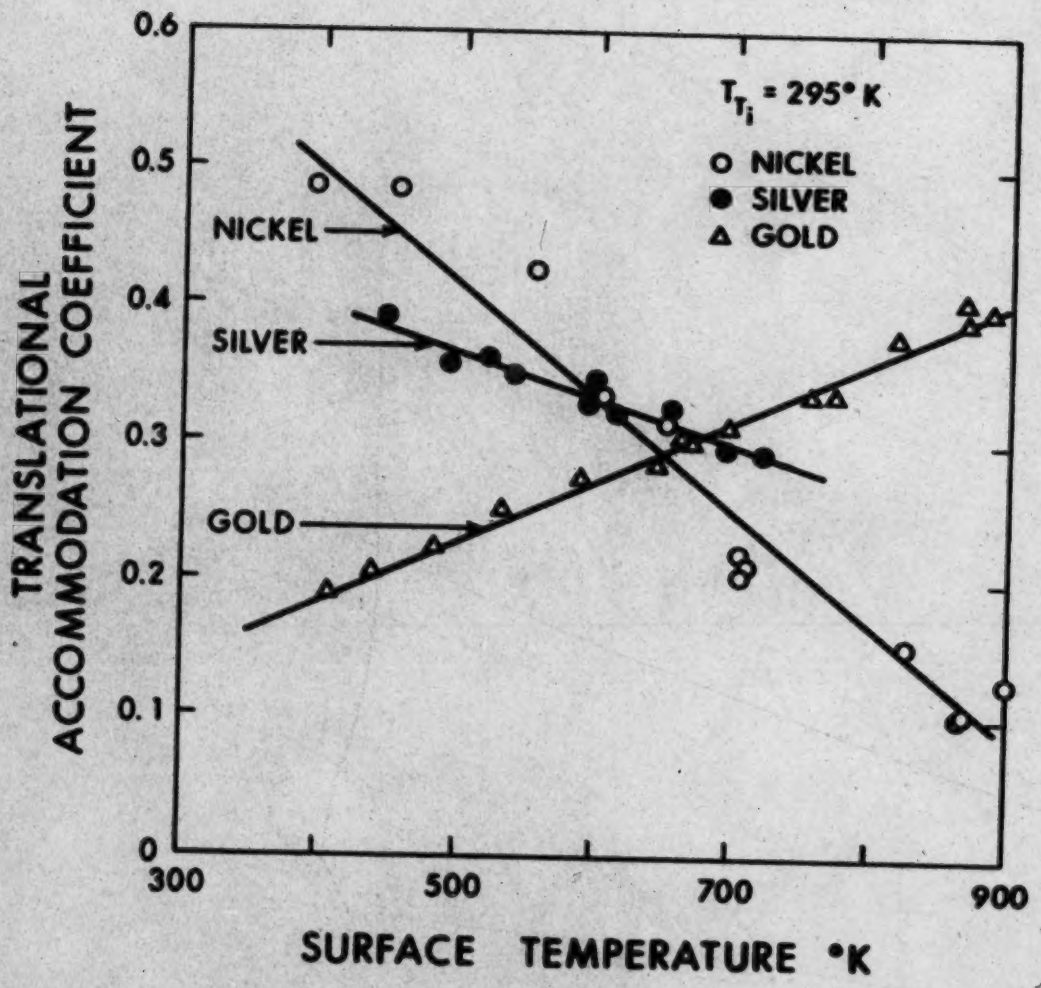

Figure 10. Variation of Translational Accommodation Coefficient of Nickel, Silver and Gold with Surface Temperature.

linear variation between α_T and T_s, the slope $d\alpha_T/dT_s$ being given by equation 5.5.

Some data which support the behaviour of α_T predicted by equation 5.5 is given now. Carpenter, Humphries and Mair (15) have reported results which show the slope $d\alpha_T/dT_s$ for nitrogen on tungsten to be 2.6×10^{-4}, while equation 5.5 gives the slope as 3.38×10^{-4} for the same conditions.

Results of Roach and Thomas (27), using the temperature jump-method, show the slope to be positive for neon and helium on tungsten, as predicted by the equation, though the magnitude of the slopes do not show agreement. There is however, good agreement for argon, the slope predicted by the equation for argon being $- 0.47 \times 10^{-4}$ and the results giving a slope of $- 0.38 \times 10^{-4}$.

Results of Thomas (28) using the low pressure method, show the slope to be $- 7.7 \times 10^{4}$ for mercury on platinum. The equation predicts the slope to be $- 11.1 \times 10^{-4}$. The results are for mercury which was not strenuously cleaned and Thomas states that the results are probably for mercury on an adsorbed film of mercury. The accommodation coefficient is probably high at higher temperatures due to evaporation of the adsorbed molecules.

Equation 5.5 gives good agreement with results obtained in this experiment for nitrogen on a variety of metals, but when applied to other combinations such as helium on tungsten, it gives values of $d\alpha_T/dT_s$ which are too large. It would appear that the constants in equation 5.5 are functions of parameters other than T_s. Equation 5.6 is proposed to

replace equation 5.5.

$$d\alpha_T/dT_s = \frac{\gamma+1}{\gamma(\gamma-1)}\left(\frac{\pi}{3}\right)^3 \frac{M}{10^5}\left|\frac{e^{\gamma/8}}{(\pi+2)\, e^{\sqrt{T_{T_i}}/\pi M}}\ \frac{1}{\mu}\ -1\right| \qquad 5.6$$

This equation satisfies the results of the present experiments and agrees well with most of the experimental results cited previously. Since not many results are available in literature showing the variation of α_T with T_s, a better check on its validity could be made if it were to be integrated to give α_T directly as a function of T_s and other known parameters, such that

$$\alpha_T = (d\alpha_T/dT_s)\ T_s \ - \ \text{Constant} \qquad 5.7$$

where the constant of integration is independent of T_s. The constant was determined by fitting equations 5.6 and 5.7 to experimental data given by Thomas (29), for helium, argon, and krypton on clean tungsten and bulk potassium. The resulting expression is given by equation 5.8

$$\text{Constant} = \frac{10^{-5}}{32}(61.19M-12525.2\sqrt{M} + 28451.63)(32+\gamma^3(\gamma+1)(1.67-\gamma)M-M_s)$$
$$+10^{-5}\ (62.07\sqrt{M} - 5.6224M - 99.47 - \frac{M(184-M_s)}{2M-10.85\sqrt{M}+33.6})$$
$$(T_{T_i} - 84.45\sqrt{M} + 4.7583M + 342.87) \qquad 5.8$$

In this expression, the ratio of the specific heats were used to make it fit the results of the present work for diatomic nitrogen.

The real test of empirical equations such as those given by equations 5.6 to 5.8 is how well they predict results for a wide range of gas-surface combinations and conditions, other than those used to determine the constant. This is discussed below for monatomic, diatomic, and polyatomic gases separately.

Monatomic gases:

The table below shows some of the results predicted by the equations. These have been compared to experimental results given by Thomas(29). The difference between surface and gas temperatures have been taken to be 17°K.

TABLE 3

Predicted accommodation coefficients for monatomic gases

Combination	T_{T_i} °K	α_T(predicted)	α_T(measured)
Xe/W	153	.86	.89
	193	.81	.85
	243	.75	.81
	303	.68	.77
He/Na	78	.041	.035
	90	.045	.038
	195	.067	.065
	298	.089	.09
A/Na	78	.45	.43
	90	.44	.39
	195	.42	.43
	298	.4	.46
He/Ni	100	.044	.048
	200	.057	.059
	300	.072	.072

The experimental results for helium on nickel are taken from Goodman's (4) paper. It appears from the table 3 that the equations predict good results for the gas-surface combinations given there. It was found, however, that for neon on tungsten they give α_T varying from 0.2 to 0.14 for a temperature range of 153° to 303°. These values are much higher than those given by Thomas (29) for the same conditions but are about half those predicted by Goodmans (4) original simple cubic lattice theory.

It can be stated in general then, that the equations work well for a large range of gas-surface combinations for monatomic gases, neon excepted.

Diatomic gases:

As stated before the equations have been adjusted to give an excellent description of the results obtained here for nitrogen on gold, silver and nickel. Of the other gases tested with the equation, hydrogen on platinum gave values of α_T varying from 0.17 at 100° to 0.2 at 600°K, the temperature of the surface being 17° higher. Though the trend of α_T versus T_{T_i} is opposite to that shown by curves 7 and 9 of figure 2 of Thomas' (28) paper, the overall values compare well. Oxygen on platinum, on the other hand, gave values of α_T which were lower than those given by Thomas (28), varying between 0.42 at 100°K to 0.22 at 400° compared to about 0.5 at 400°. Weinberg and Merrill's (30) experiments have shown that platinum behaves like nickel when reflecting light gases such as helium and like silver when reflecting heavier gases such as argon and this may explain the discrepancy between measured and

predicted results in this case. It is unfortunate that dependable results for other metals are not available in literature.

Polyatomic gases:

The only gas tested with the equation in this category was carbon dioxide. The equation predicts α_T on platinum to be 0.45 at 300°K and 0.33 at 400°K, compared to 0.48 at 300°K and 0.36 at 400°K given by Thomas (28). At higher temperatures, however the experimental results are higher than those predicted.

Obviously equations 5.6 to 5.8 need to be checked more thoroughly before their validity is established, but the results given here are deemed sufficient to support the proposition that α_T varies linearly with T_s according to equation 5.5.

5.4 Estimation of Accuracy of Measured Translational Accommodation Coefficient

From theory, equation 4.17 gives

$$\alpha_T = \left|\left|(I_2 - I_1)^2_{T_{T_i}} / (I_2 - I_1)^2_{T_{T_r}}\right| - 1\right| / (T_{s/T_{T_i}} - 1) \qquad 4.17$$

The temperatures T_s and T_{T_i} were measured by calibrated thermocouples and the error in them is not expected to be more than $\pm 1°K$.

Experiments conducted with $T_s = T_{T_i} = 295°K$ (room temperature) indicated that the scatter in $(I_2 - I_1)^2_{T_{T_i}}$ was $\pm$ 1%. Since there is no reason to expect $(I_2 - I_1)^2_{T_{T_r}}$ to be any different the scatter in it will be assumed to be $\pm$ 1%. Scatter in $(I_2 - I_1)^2_{T_{T_i}} / (I_2 - I_1)^2_{T_{T_r}}$ is calculated below, based on this.

Let $q = (I_2 - I_1)^2_{T_{T_i}}$,

$r = (I_2 - I_1)^2_{T_{T_r}}$ and $p = q/r$

Then an error in p can be written as

$$\Delta p = \frac{\Delta q}{r} - \frac{q}{r^2} \Delta r \qquad 5.9$$

where $\Delta q/q = \Delta r/r = \pm 0.01$ as noted before.

Results of a typical run gave values of $q = 163^2$ units and $r = 138^2$ units corresponding to $T_s = 790°K$.

Substituting these values

$$\Delta p = \frac{163^2}{138^2} \times 0.01 + \frac{163^2 \times 138^2}{138^2 \times 138^2} \times 0.01 = 0.03 \qquad 5.10$$

Then α_T can be written as

$$\alpha_T = (p + \Delta p - 1)/(T_{s/T_{T_i}} - 1) = \alpha_T \pm 0.03/(T_{s/T_{T_i}} - 1) \qquad 5.11$$

This variation is plotted on Figure 9. It is evident that the results fall within this probable error.

It should be noted here that $(I_2 - I_1)_{TT_i}$ is measured only once for each set of experimental runs. Hence, the values of α_T at various T_s will be affected to the same extent by the error in this variable in each run.

For each run p can be written as $p = q/r$, where q is constant.

Then $$\Delta p = \frac{q}{r^2} \Delta r \qquad 5.12$$

Substituting values indicated before

$$\Delta p = \frac{163^2}{138^2} \times \frac{138^2}{138^2} \times 0.01 = 0.0125$$

Then α_T can be written as

$$\alpha_T = \alpha_T \pm 0.0125/(T_s /T_{T_i} - 1) \qquad 5.13$$

Therefore values of α_T for each experimental run have a probable error $\pm 0.0125/(T_{s/T} - 1)$, when their magnitudes at different T_s are compared to each other. In other words, the slope $d\alpha_T/dT_s$ is more accurate than the absolute value of α_T.

Throughout this work α_T and α_R have been defined on the basis of temperatures. Such a definition assumes that both the incident and the reflected gas are in equilibrium. The justification for making such

an assumption is as follows. Equation 4.10 is derived from equation 4.9 which depends on Maxwellian distribution of the molecules. It has been stated previously that a plot of $\ln\left|I(K')/(K' + K''+1)[G](\frac{\nu}{\nu_o})^4\right|$ against $K'(K' + 1)$ will result in a straight line only if the gas has an equilibrium rotational energy distribution. Figure 7 shows such a plot and is typical of the results obtained during the experiments. It can be seen from the figure that a straight line is obtained, confirming equilibrium distribution of the rotational energy. This justifies the use of temperatures to define the rotational accommodation coefficient as in equation 1.6. With regard to the translational energy distribution, the incident gas molecules are in Maxwellian distribution. Hence, whether they are reflected diffusely or specularly the number reflected in various directions should still correspond to equilibrium distribution. The results of molecular beam experiments carried out by various authors indicate that the velocities of the reflected molecules also retain equilibrium distribution. For these reasons equation 1.5 defining α_T based on temperatures is expected to be well justified.

5.5 Surface Conditions

The values of both translational and rotational accommodation coefficients are dependent on the surface conditions. Measurements of energy accommodation by molecular heat transfer methods have shown that adsorped gas layers can change the thermal accommodation by a factor of 10.

Wachman (12) has reported 0.02 values of thermal accommodation coefficient of helium on clean tungsten, 0.185 for helium on tungsten with gas layers. No data is available indicating the effect of gas layers on the rotational coefficient.

To obtain results for clean metals, efforts were made to conduct tests on surfaces which were (a) pure as far as material composition was concerned and (b) free from adsorped gas layers during the experiment. The composition of nickel, silver and gold sheets used for target material are given in Table 4, as supplied by the manufacturer.

Table 4
Typical Analyses of Surface Material Composition

Fine Gold	Fine Silver	Nickel
Au 99.99%	Ag 99.9%	Ni 99.9%
Copper .005%	Cu .09%	C .01%
Silver .001%	Pb .03%	Mn .001%
	Fe .005%	Fe .01%
	Ni .002%	S .001%
	Zn .005%	Si .001%
	Cd .005%	Cu .01%
	Al .005%	Mg .002%
	Bi .01%	
	Total Other .06%	

The steps taken to keep the surface clean have been detailed in experimental procedure. All the experiments were conducted at high temperatures, and at these temperatures no gas layers are expected to be physically adsorbed. As far as chemical adsorption goes, Table 5, taken from Lewin (33), shows that at room temperature silver is inactive but nickel and gold are active.

Table 5

Chemical Adsorption

Metal	N_2	H_2	CO	C_2H_4	C_2H_2	O_2	CO_2	CH_4
Ag	N	N	N					
Au	N	N	N	Y	Y	N		
Ni	N	Y	Y	Y	Y	Y		N

where Y indicates chemical adsorption and N indicates none.

Oil from the diffusion pump is the likely source of most of the hydrocarbons. Two cold traps on the roughing pump line as well as the length of the pump line are expected to prevent oil vapours from getting into the system. H_2 and O_2 are formed by dissociation of water vapour in places where high temperatures are generated such as near the ionization gauge. Baking of the vacuum system should exclude most of the water vapour. On the basis of this discussion it is expected that the results are for clean metal surfaces.

CHAPTER VI

CONCLUSIONS

1) A technique for the simultaneous measurement of rotational and translational accommodation coefficients of nitrogen on a variety of solid surfaces has been developed. Reliable and repeatable results have been obtained with an accuracy of

$$\alpha_T = \alpha_T \pm 0.03/(T_s/T_{T_1} - 1) \text{ and } \alpha_R = \alpha_R \pm 0.04(\alpha_R + T_{R_1}/(T_s - T_{R_1}))$$

2) Values of α_R were appreciably less than α_T, in agreement with theory, but the absolute values are much greater than might be expected from the few theoretical results that predict quantitative values. They also showed little variation with T_s.

3) Values of α_T, on the other hand, varied with T_s. Results from three metals, nickel, silver and gold could be correlated by the equation

$$d\alpha_T/dT_s = 13.7278 \times 10^{-4} + 2.6042 \times 10^{-4}/\mu$$

Integrating this equation and adjusting the constant of integration using available experimental data, the resulting closed form solution for translational accommodation coefficient α_T,

$$\alpha_T = \frac{(\gamma+1)}{\gamma(\gamma-1)} \left(\frac{\pi}{3}\right)^3 \frac{M}{10^5} \left| \frac{e^{\gamma/8}}{(\pi+2)e^{\sqrt{T_{T_1}}/\pi M}} \frac{1}{\mu} - 1 \right|$$

$$- \frac{10^{-5}}{32}(61.19M - 12525.2\sqrt{M} + 28451.63)(32 + \gamma^3(\gamma+1)(1.67-\gamma)M-M_s)$$

$$- 10^{-5} \left| 62.07\sqrt{M} - 5.6224M - 99.47 - \frac{M(184-M_s)}{2M-10.85\sqrt{M}+33.6} \right|$$

$$\left| T_{T_1} - 84.45\sqrt{M} + 4.7583M + 342.87 \right|$$

not only gives an excellent description of the results obtained here, but also predicts correctly for a large range of gas-surface combinations and conditions.

The proposition that the translational accommodation coefficient varies linearly with surface temperature appears to be valid.

4) As α_T can be measured by this method for other gases and surfaces, it would be interesting to check the above equation for gas-surface combinations such as helium, and argon on various surfaces. One of the advantages of the present technique is that it places few restrictions on the material of the surface.

5) High temperatures of the surface can be employed. Theoretical error analysis shows that the accuracy increases as the difference in temperature between the gas and the surface increases.

6) Absolute pressure measurements are not required. This not only facilitates the performance of the experiments but also adds to the inherent accuracy.

BIBLIOGRAPHY

1. Smoluchoski M.S., On Conduction of Heat by Rarefied Gases, Phil. Mag. and Jour. Sci., Vol. 46, 5, 192, 1898
2. Stickney R.E., Momentum Transfer Between Gas Molecules and Metallic Surfaces in Free Molecule Flow, Phys. Fluids, Vol. 5, 1617, 1962
3. Loeb L.B., The Kinetic Theory of Gases, Third Edition, Dover Publications Inc. 1961
4. Goodman F.O., On The Theory of Accommodation Coefficients V. Classical Theory of Accommodation Coefficients and Trapping, "Rarefied Gas Dynamics" (Ed. J.H. de Leeuw) 1964
5. Logan R.M. and Stickney R.E., Simple Classical Model For The Scattering of Gas Atoms From A Solid Surface, J. Chem. Phys. Vol. 44, No. 1, 1966
6. Logan R.M. and Keck J.C., Classical Theory For The Interaction of Gas Atoms With Solid Surfaces, J. Chem. Phys. Vol. 49, No. 2, 860, 1968
7. Oman R.A., Calculations of The Interactions of Diatomic Molecules With A Solid Surface, "Rarefied Gas Dynamics", Suppliment 4, Vol. 1, 83, 1967
8. Feuer P., Theory Of Thermal Accommodation Coefficients For A Diatomic Gas, J. Chem. Phys. Vol. 39, No. 5 1311 1963.

9. Marsh T., The Free-Molecules Flow of Polyatomic Gas, College of Aeronautics, Cranfield, Rep. No. 159, 1963

10. Feuer P. and Osburn C. Quantum Theory of Accommodation Coefficients of Light Diatomic Gases, "Rarefied Gas Dynamics", Suppliment 5, Vol. 2, 1095, 1969

11. Allen R.T. and Feuer P., Quantum Theory of The Thermal Accommodation Coefficient and the Effect of Two Quantum Transitions, "Rarefied Gas Dynamics", Suppliment 4, Vol. 1, 109, 1967

12. Wachman H.Y., The Thermal Accommodation Coefficient, A Critical Survey, A R S Journal, Vol. 32, No. 1, 2, 1962

13. Sasaki N., Taku K., and Mitani K., The Exchange Efficiencies Of The Translational and Internal Energy of Gas Molecules on Solid Surfaces. I. Measurement by Means of Molecular Beams, Memoirs of the College of Science, University of Kyoto, A, XXV, 1949

14. Sasaki N. and Mitani K., The Exchange of Efficiencies of the Translational and Internal Energy of Gas Molecules on Solid Surfaces. II. Measurement by Means of a Vibration Hot Filament, Memoirs of the College of Science, University of Kyoto, A, XXV, 1949

15. Carpenter G., Humphries D.E. and Nair W.N., A New Method of Measuring Thermal Accommodation Coefficients, R.A.E. Tech. Note No. CPM. 38, 1963

16. Schafer K. and Riggert K.H., Zur Benstimuung Partieller Thermischer Akkommodation Koeffizienten, Zeitsehrift fur Electrochemie, 57, 751, 1953

17. Eucken A. and Krome H. Die Ausgestaltung Der Warmeleit Fahigkeitsmethode Zur Messung Der Molwarme Sehr Verdunter Gase Durch Gliechzeitige Bestimmung Des Akkommodations Koeffizienten, Zeit f Physik. Chem. Vol. 45(B) 175, 1940

18. Marsden D.J. Measurement of Energy Transfer in Gas-Solid Surface Interactions Using Electron Beam Excited Emission of Light, University of Toronto, U.T.I.A.S. Rep. No. 101, 1964

19. Muntz E.P. Measurement of Rotational Temperature, Vibrational Temperature, and Molecule Concentration, In Non-Radiating Flows of Low Density Nitrogen, University of Toronto, U.T.I.A. Rep. No. 71, 1961

20. Childs W.H.J., Perturbations and Rotational Constants of Some First Negative Nitrogen Bands, Proc. Royal, Soc. of London, Vol. A137, 641, 1952

21. Knudsen M., Radiometerdruck and Akkommodationkoeffizient Ann. Physik, 6, 129, 1930

22. Ashkenas H., Rotational Temperature Measurements In Electron Beam Excited Nitrogen, Phys. Fluids, Vol. 10, No. 12, 2509, 1967

23. Harbour P.J., Bienkowski G.K., Smith R.B., Influence of Secondary Electrons on an Electron-Beam Probe, Phys. Fluids, Vol. 11, No. 4, 800, 1968

24. Robben F. and Talbot L., Measurement of Shockwave Thickness By The Electron Beam Fluorescence Method, Phys. Fluids, Vol. 9, No. 4, 633, 1966

25. Lillicrap D.C. and Harvey J.K., Electron Beam Rotational Temperature Measurements Including the Effect of Secondary Electrons, A I A A Journal, Vol. 7, Part 1, 980, 1969

26. Dunn D.A. and Self S.A., Static Theory of Density and Potential Distribution in Beam Generated Plasma, J. Applied Physics, Vol. 35, No. 1, 113, 1964

27. Roach D.V. and Thomas L.B., Determination of The Thermal Accommodation Coefficients of Gases on Clean Surfaces at Temperatures Above 300°K By The Temperature Jump Method, "Rarefied Gas Dynamics", Suppliment 4, Vol. 1, 163, 1967

28. Lloyd B. Thomas., Thermal Accommodation of gases on Solids. Fundamentals of Gas-Surface Interactions. Edited by H. Saltsburg, J.N. Smith and H. Rogers, Academic Press, New York and London, 346, 1967

29. Lloyd B. Thomas., A Collection of Some Controlled Surface Thermal Accommodation Coefficient Measurements, "Rarefied Gas Dynamics", Supplement 4, Vol. 1., 155, 1967.

30. Weinberg W.H. and Merril R.P., Scattering of Helium, Neon, Argon, Krypton, Xenon and Deuterium From A Tungsten (110) Surface Characterized by Leed, J. Chem., Phys., Vol. 56 No. 6, 2881 1972

31. Muntz E.P., The Electron Beam Fluorescence Technique, Agardograph 132, 1963

32. Hertzberg G., Spectra Of Diatomic Molecules, Van Nostrand Co., (1950)

33. Lewin G., Fundamentals of Vacuum Science and Technology, McGraw-Hall Inc. 1972

APPENDIX

The mechanism of excitation of the nitrogen molecules from the ground state N_2 $X^1\Sigma$ to an ionized state by the electron beam has been given in detail by Muntz (31). Only the highlights will be mentioned below.

It has been stated in reference (19) that the limiting pressure at which a direct excitation to $N_2B^2\Sigma$ state and subsequent emission can take place, unaffected by gas kinetic collisions, is about 470×10^{-3} torr at room temperature. The pressure used in these experiments was 5 orders of magnitude lower.

In none of the experiments did the temperature of the gas exceed 800°K. Hence, there was no significant excitation of the vibrational mode (19). Figure 11 shows schematically the excitation process at the top, the emission process in the middle, and the excitation emission path voltage levels at the bottom, and is reproduced from reference (19).

The ionization, implying the carrying away of a secondary electron with a spin of 1/2, is the cause of change in multiplicity of 1 during the excitation from N_2 $X^1\Sigma$ to $N_2B^2\Sigma$. The spin coupling in the upper state is very weak, and it can be assumed that the doublet states are unresolved. The transition is assumed to belong to Hund's case (b) (32) and the applicable selection rule $\Delta J = \pm 1$, except for the spin change of 1/2 due to the removal of an electron. The rotational levels are designated $K = J \pm 1/2$ and the selection rule, then $\Delta K = \pm 1$, gives

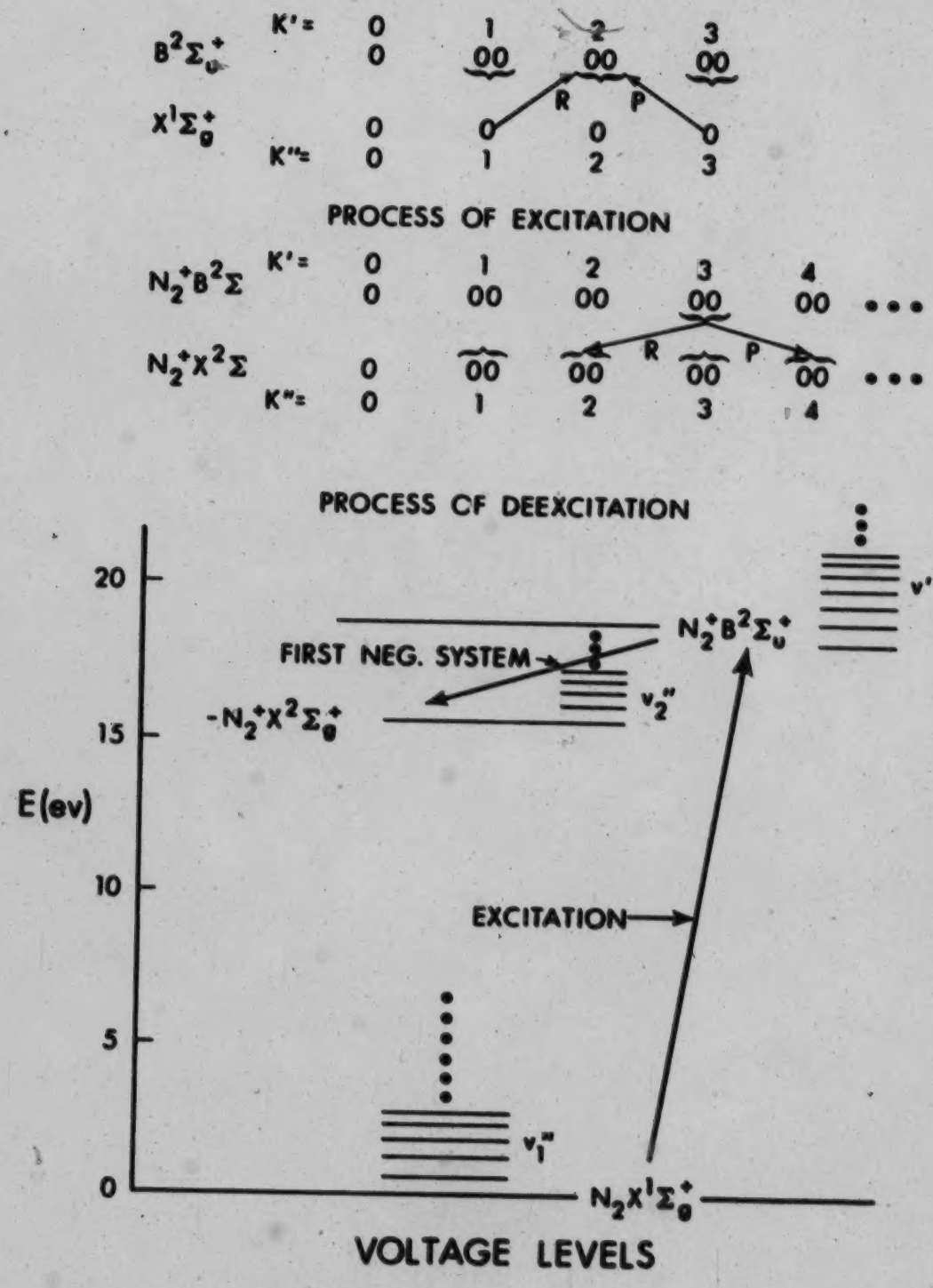

Figure 11. Mechanism of Fluorescence.

two paths of excitation, P and R, as shown in Figure 11 (top) corresponding to populating of energy level K' of the upper state from two levels of the ground state whose energy levels correspond to K' $\pm$ 1. Thus, as shown in Figure 11, the rotational energy level of $N_2 B^2\Sigma$ state, K' = 2 is populated from the energy levels of the lower state N_2 $X^1\Sigma$, K'' = 1 and 3 along R and P branches respectively. $\Delta K = 0$ transitions are forbidden.

The emission process is somewhat similar to the excitation process. The transition is from $N_2 B^2\Sigma$ to N_2 $X^2\Sigma$. The middle part of Figure 11 shows the transition schematically. There is no multiplicity change and the lower state also has a very weak spin coupling. The $^2\Sigma$ to $^2\Sigma$ transition reduces the $^1\Sigma$ to $^1\Sigma$ transition, if the doublets are unresolved. This again corresponds to Hund's case (b) (32) type, and the selection rule $\Delta K = \pm 1$, will lead to P and R branches of emission.

A theoretical calculation of line intensities has been carried out by Muntz (19). This has not been reproduced here. One notable feature of the line intensities is that in the ground state N_2 $X^1\Sigma$ of the nitrogen molecule, the nuclear spin causes the odd rotational levels (K'' = 1,3,5, etc.) to have exactly half the population of the even levels (19). Selection rule $\Delta K = \pm 1$, populates the odd numbered levels in the upper state with twice as many molecules as the even numbered. This causes the peaks corresponding to K' = 1,3,5, etc. to be twice as intense as those corresponding to K' = 2,4,6, etc.

Only the R branch of emission is of interest as it is the only branch the spectrometer could resolve. The P branch forms a bandhead and turns back on itself, making it very difficult to resolve.

Given below are the wave lengths at which the peaks of the R branch occur. These values correspond to rotational energy levels K' from 3 to 15. They have been taken from a paper by Child (20). The difference in wave lengths between successive peaks in Angstrom units is also given. This forms the criterion for working out the dimensions of the slits.

Table 6
Wavelengh of peaks in the R-branch

K'	Wavelength A	Difference
3	3908.298	
4	07.533	0.765
5	06.703	0.830
6	05.841	0.862
7	04.927	0.914
8	03.969	0.958
9	02.956	1.013
10	01.915	1.041
11	00.829	1.086
12	3899.713	1.116
13	98.499	1.214
14	97.267	1.232
15	95.996	1.271

As stated, the spectrometer could resolve only this band. By resolution, it is meant that when one of the peaks is centred over the exit slit, the neighbouring peaks do not influence its intensity.

The resolving capacity of the set up was dependent mainly on three interrelated factors. The first was the inherent capacity of the spectrometer to resolve. This depends on the linear resolving power of the spectrometer and the widths of the entrance and exit slits. The details for calculating proper slit widths are given by Marsden (18) and these have been incorporated into the set up. The slit widths were a compromise between obtaining good resolution and intensity of light signal. Too large a width resulted in poor resolution and too narrow a width reduced the signal to below acceptable signal-noise ratio. The widths were set at 0.003 inches for entrance and 0.004 inches for exit slits, as these gave the best results.

The second factor affecting resolution was the speed at which the spectrometer scanned. Too fast a scan resulted in poor resolution because of the time constants inherent in the coupled electrical measuring devices. Internal friction of the scanning mechanism prevented it from being run below a certain speed.

The third factor is related to the second: the time constants of the measuring devices used, namely the electrometer and the chart recorder, and noise produced by the photomultiplier and the two above-mentioned instruments. The fluctuations in the output of the EMI 9502 S photo-

multiplier depends on the light intensity being measured. If, for example, the light intensity causes a nominal 1000 pulses per second, and this is averaged over periods of 1 second, then the root mean square of the fluctuations is statistically equal to the reciprocal of the square root of 1000 or about $\pm$3%. The greater the line intensity, the higher the number of pulses produced and the lower will be the statistical fluctuation. To integrate out this noise, a 500 mFu capacitance was inserted across the anode and the ground of the photomultiplier near the electrometer terminals.

An integrating RC circuit was inserted between the electrometer and the chart recorder. It consisted of a 10 K potentiometer and a 1 mF capacitance. The potentiometer resistance was adjusted until the noise from the electrometer was damped out. The electrometer was on 10×10^{-10} ampere scale. Its output was three volts. The chart recorder was adjusted to give full-scale deflection at two volts. It was offset to read about 1/10 of the full scale deflection when the electrometer was reading the dark current which had a value of 4×10^{-10} amperes. Power supplied to run the spectrometer scanning mechanism motor was adjusted so that the scan between peaks a K' = 1 to 17 took about 10 minutes.

A computer program was written to calculate the rotational temperature. The data supplied were the line intensities at K' = 3 to 15, as given in Table 2. The following steps were carried out by the program which is attached.

1. The temperature dependent factor [G] was calculated at T_R = 300°K for all values of K'. $\text{Ln}(I(K')/(K' + K'' + 1)[G](\frac{\nu}{\nu_o})^4)$ were then calculated. $(\frac{\nu}{\nu_o})^4$, a constant for each value of K' was stored in the program.

2. A least squares straight line was fitted to these points with K'(K' + 1) as the abscissa. From the slope of this line, T_R was calculated. If this T_R differed from 300°K by more than 25°K, the new temperature was used iteratively in step 1.

3. The variance was calculated and all points lying outside this were thrown out. Step 1, 2 and 3 were repeated until all outliers were eliminated. Then the rotational temperature, extreme temperature corresponding to the standard deviation and the percentage deviation were printed.

For purposes of checking the number of points used to define the line, the print out contained data points used, the points thrown out being printed as zeroes. A print out of the results for the case when the surface temperature is equal to room temperature is also attached.

```
      DIMENSION A(30),B(40),Y(30), X(30),
      ST(10),G(30),YCAL(30)
      READ(5,20)N,NUMBR
   20 FORMAT(2I10)
      READ(5,22)(B(I),I=1,17)
   22 FORMAT(8F10.3)
C     B(I)  WAVELENGTHS OF R-BRANCH PEAKS
      DO 2 I=1,17
      B(I)=3908.2/B(I)
      B(I)=B(I)*B(I)
      B(I)=B(I)*B(I)
      X(I)=I*(I+1)
    2 CONTINUE
C     B(I)=NEW/NEWNOT RAISED TO 4
C     X(I)=K'(K'+1)
      KOUNT=0
   52 READ(5,21)(A(I),I=3,N)
   21 FORMAT(8F10.3)
C     A(I) MEASURED LINE INTENSITIES STARTING AT K'=3
      READ(5,112)TEMP
  112 FORMAT(F10.3)
      WRITE(6,111)TEMP
  111 FORMAT(//T8, 'SURFACE TEMPERATURE, DEGREES KELVIN=',F10.3)
      Y(I)=0.
      G(I)=0
      L=0
      M=0
      T(1)=300.
      B(19)=2.00065*1.4384
C     B(19)=BV1''*HC/K'
C     BV1=ROTATIONAL CONSTANT IN GROUND STATE
C     H=PLANCK'S CONSTANT
C     C=SPEED OF LIGHT
C     K=BOLTZMANN'S CONSTANT
      K=0
    3 DO 4 I=3,N
      IF(A(I).EQ.0.)GOTO70
      IF(X(I).EQ.0.)GOTO60
      G(I)=(I+1)*EXP(-2.*B(19)*I+1)/T(1))
      G(I)=G(I)+I*EXP(2.*B(19)*I/T(1))
      G(I)=G(I)/(2.*I+1)
      G(I)=ALOG10(G(I)*B(I)
      Y(I)=ALOG10(A(I))-G(I)-ALOG10(2.*I)
      GOTO60
   70 Y(I)=0
      M=M+1
```

```
   60    WRITE(6,45)G(I),Y(I),X(I),A(I)
   45    FORMAT(/,4F10.3)
C        G(I)=(G) OF MUNTZ'S EQUATION
C        Y(I)=LOG I(K')/(K'+K''+1)(G)B(I)
    4    CONTINUE
         SUMY=0.
         SUMX=0.
         SUMXY=0.
         SUMXX=0.
         DO 5 I=3,N
         IF(A(I).EQ.0.)GOTO5
         IF(X(I).EQ.0.)GOTO5
         SUMY=SUMY+Y(I)
         SUMX=SUMX+X(I)
         SUMXY=SUMXY+(X(I)*Y(I))
         SUMXX=SUMXX+(X(I)*X(I))
    5    CONTINUE
         WRITE(6.49)SUMY,SUMX,SUMXY,SUMXX
   49    FORMAT(//,4F14.3)
   10    SUMYX=SUMY*SUMX/(N-M-L-2)
         SUMXP=SUMX*SUMX/(N-M-L-2)
         SLOPE=(SUMXY-SUMYX)/(SUMXX-SUMXP)
         CONST=SUMY-(SUMX*SLOPE)
         CONST=CONST/(N-M-L-2)
         WRITE(6.51)SLOPE,CONST
   51    FORMAT(2F10.6)
         T(2)=2.00065*1.4384/(2.302585*SLOPE)
         T(2)=ABS(T(2))
         T(3)=ABS(T(2)-T(1))
         T(1)=T(2)
         K=K+1
         IF(K.GT.7)GOTO11
         WRITE(6.40)K,T(1)
   40    FORMAT(//T8,110,'APPOROX, TEMP.=',F10.3)
         M=0
         IF(T(3).GT.25.)GOTO3
         SUM=0.
         DO 6 I=3,N
         YCAL(I)=SLOPE*I*(I+1)+CONST
         IF(A(I).EQ.0.)GOTO6
         IF(X(I).EQ.0.)GOTO6
         SUM=SUM+(Y(I)-YCAL(I))**2
    6    CONTINUE
         SIGMA=2.*(SUM/(N-M-L-2)**.5
         SIGMA=2.*SIGMA
```

```
C               SIGMA=VARIANCE
                WRITE(6,61)SUM, SIGMA
     61         FORMAT(2F10.3)
                WRITE(6,75)(YCAL(I),I=3,15)
     75         FORMAT(F10.3)
                J=N
                C=SUMY
                DO 9 I=3,N
                IF(X(I).EQ.0.)GOTO9
                IF(A(I).EQ.0.)GOTO9
                IF(ABS(Y(I)-YCAL(I)).LT.SIGMA)GOTO9
                J=J-1
                C=SUMY-Y(I)
                SUMX=SUMX-X(I)
                SUMXY=SUMXY-X(I)*Y(I)
                SUMXX=SUMXX-X(I)*X(I)
                Y(I)=0.
                X(I)=0.
                L=L+1
      9         CONTINUE
                IF(C.EQ.SUMY)GOTO11
                SUMY=C
                GOTO 10
     11         WRITE(6.25)T(1)
     25         FORMAT(//T8,'ROTATIONAL TEMPERATURE=',F10.3)
                XBAR=SUMX/(J-2)
                XSQ=0
                DO 12 I=3,N
                IF(A(I).EQ.0.)GOTO12
                IF(X(I).EQ.0.)GOTO12
                XSQ=XSQ+(X(I)-XBAR)**2
     12         CONTINUE
                SIGMA=SUM/(J-2)
                SIGSP=SIGMA/XSQ
                STDEV=SQRT(ABS(SIGSP))
C               STDEV=STANDARD DEVIATION
                T(4)=ABS((T(1)*SLOPE)/(SLOPE+STDEV))
                T(5)=ABS((T(1)*SLOPE)/(SLOPE-STDEV))
                WRITE(6,30)T(4),T(5)
     30         FORMAT(//T8,'EXTREME TEMP.=',2F10.3)
                T(4)=(T(4)-T(1))/T(1)*100.
                T(5)=(T(5)-T(1))/T(1)*100.
                WRITE(6,31)T(4),T(5)
     31         FORMAT(//T8,'PERCENTAGE TEMP. DEVIATION=',2F10.3)
                KOUNT=KOUNT+1
                DO 100 I=1,17
    100         X(I)=1*(I+1)
                IF(KOUNT.LE.NUMBER)GOTO52
```

SURFACE TEMPERATURE, DEGREES KELVIN= 295.000

-0.007	0.748	12.000	33.000
-0.006	0.712	20.000	40.600
-0.005	0.670	30.000	46.200
-0.004	0.617	42.000	49.200
-0.002	0.557	56.000	50.200
-0.001	0.487	72.000	49.000
0.001	0.411	90.000	46.500
0.003	0.323	110.000	42.400
0.005	0.232	132.000	38.000
0.008	0.125	156.000	32.600
0.010	0.015	182.000	27.600
0.013	-0.108	210.000	22.500
0.016	-0.233	240.000	18.200

4.555 1352.000 182.238 208312.000

-0.004305 0.798158

1APPOROX. TEMP.= 290.281

```
      0.000
YCAL  0.746
      0.712
      0.669
      0.617
      0.557
      0.488
      0.411
      0.325
      0.230
      0.127
      0.015
     -0.106
     -0.235
```

ROTATIONAL TEMPERATURE = 290.281

EXTREME TEMP.= 290.624 289.939

PERCENTAGE TEMP. DEVIATION = 0.118 -0.118

F05046A8	00509E38	00509BD8	00000132
00000001	00000004	00000000	00509130
43132000	00000000	43122480	00000000